Astronomy & Astrophysics manuscript no. 00000
July 24, 2018

The XMM-Newton serendipitous survey

VIII: The first XMM-Newton serendipitous source catalogue from overlapping observations⋆,⋆⋆

I. Traulsen[1], A. D. Schwope[1], G. Lamer[1], J. Ballet[2], F. Carrera[3], M. Coriat[4], M. J. Freyberg[5], L. Michel[6], C. Motch[6], S. R. Rosen[7], N. Webb[4], M. T. Ceballos[3], F. Koliopanos[4], J. Kurpas[1], M. Page[8], and M. G. Watson[7]

[1] Leibniz-Institut für Astrophysik Potsdam (AIP), An der Sternwarte 16, 14482 Potsdam, Germany
e-mail: itraulsen@aip.de
[2] AIM, CEA, CNRS, Université Paris-Saclay, Université Paris Diderot, Sorbonne Paris Cité, F-91191 Gif-sur-Yvette, France
[3] Instituto de Física de Cantabria (CSIC-UC), Avenida de los Castros, 39005 Santander, Spain
[4] IRAP, Université de Toulouse, CNRS, UPS, CNES, 9 Avenue du Colonel Roche, BP 44346, 31028 Toulouse Cedex 4, France
[5] Max-Planck-Institut für extraterrestrische Physik, Giessenbachstraße 1, 85748 Garching, Germany
[6] Observatoire astronomique, Université de Strasbourg, CNRS, UMR 7550, 11 rue de l'Université, 67000 Strasbourg, France
[7] Department of Physics & Astronomy, University of Leicester, Leicester, LE1 7RH, UK
[8] Mullard Space Science Laboratory, University College London, Holbury St Mary, Dorking, Surrey RH5 6NT, UK

Received July 24, 2018; accepted ...

ABSTRACT

Context. XMM-Newton has observed the X-ray sky since the beginning of 2000. The XMM-Newton Survey Science Centre Consortium has been publishing catalogues of X-ray and ultraviolet sources found serendipitously in the individual observations. This series is now augmented by a catalogue dedicated to X-ray sources detected in spatially overlapping XMM-Newton observations.
Aims. This catalogue aims at exploring repeatedly observed sky regions. It thus makes use of the long(er) effective exposure time per sky area and offers the opportunity to investigate long-term flux variability directly through the source detection process.
Methods. A new standardised strategy for simultaneous source detection on multiple observations is introduced, including an adaptive-smoothing method to describe the image background. It is coded as a new task edetect_stack within the XMM-Newton Science Analysis System and used to compile a catalogue of sources from 434 stacks comprising 1 789 overlapping XMM-Newton observations that entered the 3XMM-DR7 catalogue and have a low background and full-frame readout of all EPIC cameras.
Results. The first stacked catalogue is called 3XMM-DR7s. It contains 71 951 unique sources with positions and source parameters like fluxes, hardness ratios, quality estimate, and information on inter-observation variability, which are directly derived from a simultaneous fit and calculated for the stack and for each contributing observation. More than 8 000 sources are new with respect to 3XMM-DR7. By stacked source detection, the parameters of repeatedly observed sources can be determined with higher accuracy than in the individual observations. It is more sensitive to faint sources and tends to produce fewer spurious detections.
Conclusions. With this first catalogue we demonstrate the feasibility and benefit of the approach. It supplements the large data base of XMM-Newton detections by additional, in particular faint, sources and new variability information. In the future, it will be expanded to larger samples and continued within the series of serendipitous XMM-Newton source catalogues.

Key words. catalogs – astronomical databases: miscellaneous – surveys – X-rays: general

1. Introduction

ESA's X-ray mission, XMM-Newton (Jansen et al. 2001), was launched in December 1999 and is dedicated to pointed X-ray and ultraviolet to optical observations. Its large field of view and effective area make it also suitable for survey-like searches for serendipitous X-ray detections. Up to one hundred are found in addition to the main target in an XMM-Newton observation with the EPIC CCD instruments pn (Strüder et al. 2001), MOS1, and MOS2 (Turner et al. 2001). The XMM-Newton Survey Science Centre Consortium (SSC, Watson et al. 2001) has been generating catalogues of individual detections, merged into unique sources, from public XMM-Newton observations since the beginning of the mission. The series of XMM-Newton Serendipitous Source Catalogues are produced from pointed observations with the EPIC instruments. The most recent data release 3XMM-DR8 of the 3rd catalogue generation has been published on May 16th, 2018. The catalogue series and the underlying software are described by Watson et al. (2009, hereafter: Paper V) and Rosen et al. (2016, hereafter: Paper VII). Complementary source catalogues are the Slew Survey Source Catalogue (Saxton et al. 2008) from EPIC-pn data taken during telescope slews and the XMM-Newton OM Serendipitous Ultraviolet Source Survey Catalogue (Page et al. 2012) from data taken with the Optical Monitor. The software to reduce and analyse XMM-Newton data and to compile the catalogues has been developed by the SSC

⋆ Based on observations obtained with XMM-Newton, an ESA science mission with instruments and contributions directly funded by ESA Member States and NASA.
⋆⋆ The catalogue is available as FITS file via the SSC web pages at https://xmmssc.irap.omp.eu and searchable via XCatDB https://xcatdb.unistra.fr/3xmmdr7s and XSA https://www.cosmos.esa.int/web/xmm-newton/xsa.

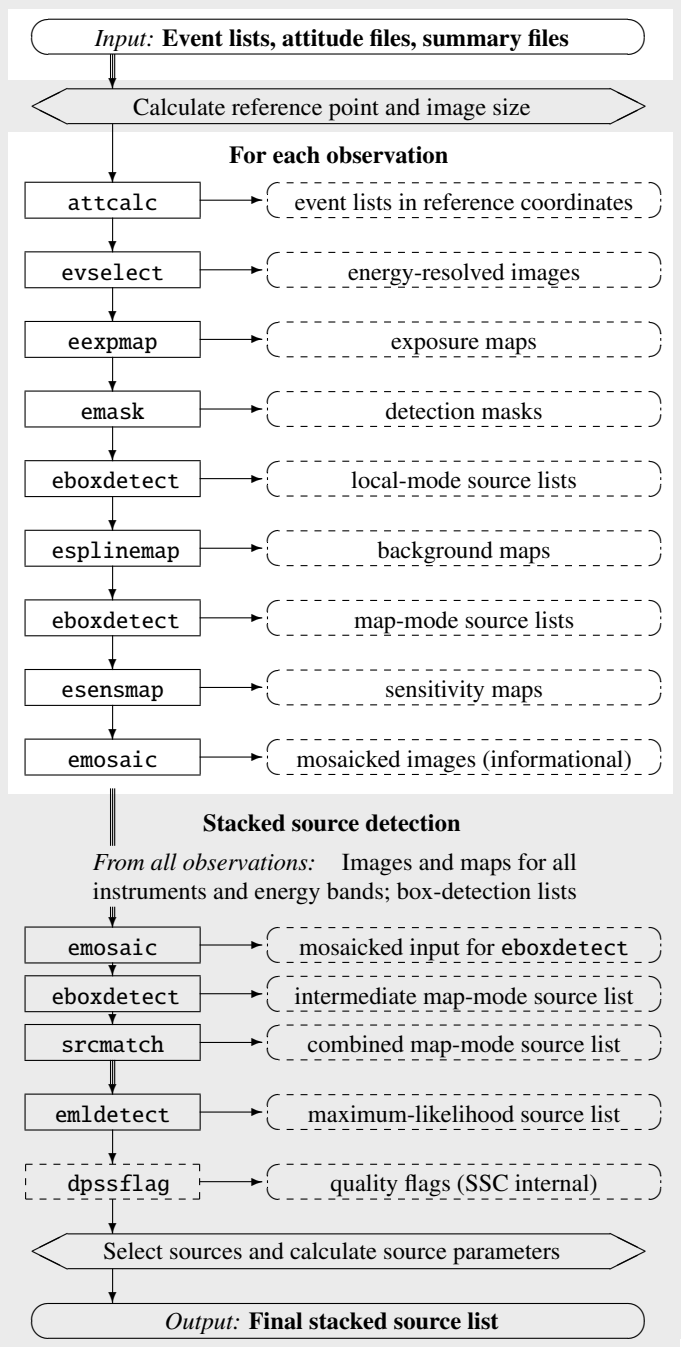

Fig. 1. Structure of `edetect_stack`. Internal steps are listed in hexagonal boxes, calls to external SAS tasks in rectangular boxes, and their data products in dashed rounded boxes. Task stages dealing with all observations simultaneously are highlighted by grey background.

and the XMM-Newton Science Operations Centre (SOC) and is released regularly by the SOC.

After seventeen years in orbit, XMM-Newton has re-observed many patches of the sky. Overall, almost a third of the XMM-Newton sky has been visited more than once. This may occur from planned, repeated observations of variable or calibration targets, mosaicked observations of large regions, or unplanned overlaps of the fields of view of neighbouring independent observations. To properly exploit the survey potential of the growing body of multiply-imaged sky areas in the XMM-Newton archive, we have now developed a new standardised approach to source detection in multiple observations. A maximum likelihood fitting algorithm in the five standard energy bands *(1)* 0.2−0.5 keV, *(2)* 0.5−1.0 keV, *(3)* 1.0−2.0 keV, *(4)* 2.0−4.5 keV, and *(5)* 4.5−12.0 keV is employed similar to the source-detection method used to produce the other XMM-Newton source catalogues. Parameters of each source are derived from overlays of the empirical point spread functions depending on the instrument, energy band, and off-axis position. The full procedure from the input event lists to the final stacked source list has been made available to all users as a new task edetect_stack of the XMM-Newton Science Analysis System software.

This paper, number VIII in the series of publications dedicated to the catalogues of serendipitous detections in XMM-Newton pointing-mode observations, introduces the first catalogue of X-ray detections on spatially overlapping EPIC observations. Being the first release using stacked source detection, it also serves as a method validation and as a feasibility study. It has been compiled from a selection of good-quality data, namely 3XMM-DR7 observations with large usable chip area and reasonably low background. Within the series of XMM-Newton serendipitous source catalogues, it is named 3XMM-DR7s.

The following paper Section describes the data processing and source detection on multiple observations, an implementation of an adaptive smoothing technique to model the background in the images, and the detection efficiency and sensitivity for overlapping observations. Section 3 contains the selection criteria of the observations that enter the first stacked catalogue and a new strategy to identify observations with high background emission throughout the exposure time. Section 4 covers the compilation of the catalogue, its properties, and the options to access it and the auxiliary products. Section 5 gives information on planned future catalogue versions and a summary.

2. Data processing and source detection

The new catalogue 3XMM-DR7s is based on archival XMM-Newton data that entered 3XMM-DR7. Throughout the paper, we refer to it as the stacked catalogue and to the other data releases from source detection on single observations as the 3XMM catalogues. The term "stack" is used for a group of overlapping observations for which simultaneous source detection is performed. In the context of XMM-Newton observations, the term "exposure" stands for the measurement by one of its instruments within an observation. "Images" are created for each observation, instrument, and energy band separately, if not noted otherwise. If several images are merged into a single file, it is called a "mosaic".

3XMM-DR7s is processed with the XMM-Newton Science Analysis Software (SAS, Gabriel et al. 2004) version 16 and calibration files as of July 2017. We follow the data handling outlined in Papers V, VII, and the 3XMM-DR4 online documentation[1], using the same parameters as in the 3XMM pipeline wherever applicable. The tasks are adjusted to the needs of source detection on multiple observations, including the handling of many input files and large image sizes, runtime improvements, wider ranges of allowed parameter values than in single observations, e.g. the minimum detection likelihood, and additional output used to create the final stacked source list. The new standardised approach to perform stacked source detection on multiple observations has entered the SAS as a new task `edetect_stack` together with the updates to the existing source-detection tasks. Its structure is illustrated in Fig. 1. It is a combination of newly

[1] `https://xmmssc-www.star.le.ac.uk/Catalogue/3XMM-DR4/UserGuide_xmmcat.html`

written Perl code and up to eleven other SAS tasks, comprising three major steps: *(i)* Input data to source detection are prepared for each observation individually (described in the next two subsections). All input images are created with the same binning, reference coordinates, and size, large enough to cover the observed sky areas of all observations in the stack. *(ii)* Source detection is run on all input data simultaneously (described in Sect. 2.3) and the results per input image are stored in an intermediate source list. In both steps, `edetect_stack` determines the appropriate parameter values for the other SAS tasks and calls them. *(iii)* Sources which enter the final source list are selected and their source parameters calculated from the results of the previous step. For source detection on a single observation, this step is part of the task `emldetect`. For source detection on multiple observations, modifications are needed and a module of `edetect_stack` refines this functionality of `emldetect` (described at the end of Sect. 2.3).

2.1. Preparation of the input data for maximum-likelihood source detection

Event lists and attitude files to produce the new catalogue are taken from the set of files used to produce the XMM-Newton Serendipitous Source Catalogues 3XMM-DR5 to DR7. Within the pipeline processing, the event lists are filtered for good time intervals (GTIs) per CCD with a minimum GTI length of 10 s, cleaned of bad pixels and merged per instrument. They are publicly available via the XMM-Newton Science Archive (XSA[2]). For the 3XMM catalogues, time intervals of background flares are identified in the merged event lists for each instrument using an optimised flare filtering method. Observations in mosaic mode have been split into sub-pointings and attributed individual observation identifiers. More details on the pipeline can be found in Paper VII. For the stacked catalogue, the XSA event lists are filtered with all 3XMM GTIs. If two event lists per instrument are available with the same observation identifier ("scheduled" part of the observation with exposure identifier "S" and "unscheduled" part with exposure identifier "U"), they are combined using the task `merge`. Within `edetect_stack`, information about the telescope boresight during the exposure time is obtained from the attitude files. Therefore, they are also filtered with the combined GTIs of all EPIC instruments for the stacked catalogue to eliminate erroneously recorded coordinate shifts.

The filtered event lists and attitude files of a stack of observations are passed to the task `edetect_stack`. It establishes a common coordinate system for the stack from the pointing coordinates in the attitude files, which is used for all subsequent source-detection steps. The events are projected onto reference coordinates in the local tangent plane using the task `attcalc`[3]. The reference point of the projection is calculated as the average of the minimum and maximum coordinates of all overlapping observations. The size of the sky area covered by them is derived from their pointing coordinates and position angles. Using the projected event lists, the input files for source detection are prepared for each contributing observation individually, namely images and corresponding exposure maps, detection masks, and background maps for the three EPIC instruments and the five 3XMM energy bands over the full sky area of the stack. The images are created in bins of $4'' \times 4''$ by the task `evselect`. Exposure maps are created by `eexpmap` and give the exposure time per instrument, taking invalid pixels and relative detector efficiency into account. They serve as input to the detection masks and background maps. For the source-detection tasks, a second set of exposure maps is produced taking vignetting corrections into account. Detection masks are created by `emask` for each instrument and give the valid pixels per image. They are derived from the lowest energy band, which defines the most conservative mask. Background maps are created by `esplinemap` and give the modelled background counts per pixel. Their production is described in more detail in the next subsection. In addition to these mandatory input files for source detection, two sets of standard data products are created for purely informational purposes: Sensitivity maps are calculated by `esensmap` per instrument and energy band. All input images and those per energy band are combined into mosaics by `emosaic` to illustrate the stacks.

2.2. Modelling the EPIC background by an adaptive smoothing technique

The EPIC background includes an internal instrumental background and external components such as the cosmic X-ray background together with a time-variable local particle background linked to the complex interaction of solar activity with the Earth's magnetosphere (e.g. Read & Ponman 2003). For source detection, time intervals dominated by high and variable background are filtered from the 3XMM-DR7 event lists (see Sect. 3.2.3 of Paper VII). The remaining background is modelled based on source-excised ("cheesed") images by the task `esplinemap` and used within the source-detection tasks. To construct the cheesed images, sliding-box source detection is performed on the input images by the task `eboxdetect`, run in the so-called local mode. The resulting list of tentative source positions is passed to the task `esplinemap`, which excludes circular regions centred at the listed positions within a brightness-dependent radius from each input image. A spline fit has been the standard method to model the background and extrapolate it to the source positions in single observations, also employed for the 3XMM catalogues. It gives a reasonably good description of the background behaviour in most images of standard size from single pointings. Test runs, however, have revealed that its current SAS implementation can result in undesired overshoot or ringing effects for images that are larger than a single XMM-Newton EPIC field of view as needed for stacked source detection. The artifacts occur in particular close to the sharp transition between the exposed and the un-exposed image area within and outside the single field of view. Furthermore, the splines may smooth out small-scale variations in very complex background structures. Thus, an adaptive filtering method to model the background emission has been introduced in `esplinemap`[4] as an alternative to the spline fitting. The cheesed images, normalised by the exposure maps, and the corresponding masks are smoothed by convolving them with a Gaussian kernel. To account for different background structures in individual images and image areas, an optimum smoothing radius is determined pixel by pixel such that the final adaptively smoothed background image has a uniform signal-to-noise ratio over all pixels, which limits the allowed noise fluctuations in the output. Therefore, the initial width of the Gaussian kernel is increased by a factor of $\sqrt{2}$ in eight steps. The counts per pixel in the smoothed images are the

[2] `https://www.cosmos.esa.int/web/xmm-newton/xsa`

[3] The maximum area distortion introduced by tangential projection in the images used for the stacked catalogue with side lengths up to 4° is smaller than 4×10^{-3} and thus negligible in source detection.

[4] Although the task is now capable of three different methods of background modelling including spline fits and smoothing, its initial name `esplinemap` is retained to be consistent with former SAS versions.

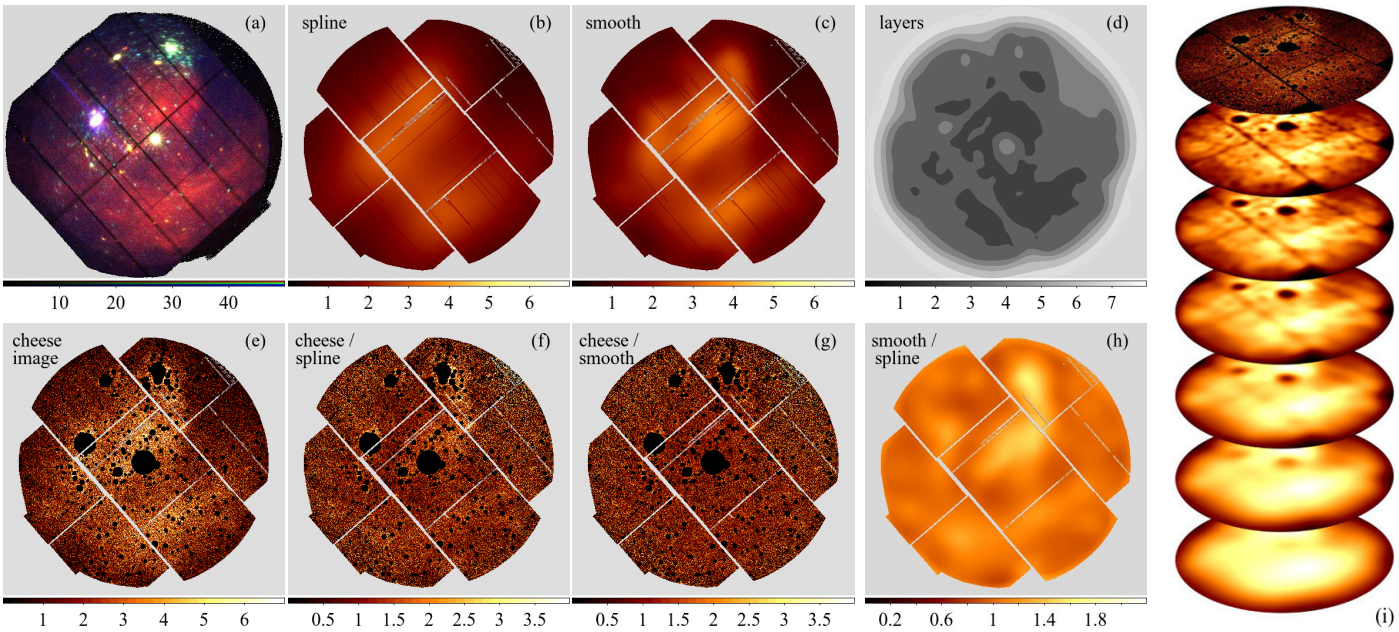

Fig. 2. Different methods of background modelling, illustrated on the example of an observation of the η Carinae region (observation identifier 01125670101). The panels include a three-band false-colour image of the EPIC observation (0.2–1.0 keV, 1.0–2.0 keV, 2.0–12.0 keV), showing *(a)* the complex background structure of the field, *(b)* the MOS1 background map derived from a spline fit and *(c)* from adaptive smoothing, *(e)* the cheesed image, *(f)* and *(g)* its ratio to the two background maps and *(h)* the ratio between them. The cheesed image is smoothed with a Gaussian kernel of increasing width *(i)*. All images have a linear intensity scale. The smoothed layers which are chosen per image pixel to construct the background map according to their signal-to-noise ratio are shown in grey-scale *(d)*.

weighted average over the kernel extent centred at the pixel position. Their Poissonian signal-to-noise ratio is calculated as the square root of the counts under the kernel. For each image pixel, the two smoothed images with the signal-to-noise ratios closest to the pre-defined (user-supplied) optimum are selected. The background value with the desired optimum signal-to-noise ratio in the pixel is linearly interpolated between them. Small-scale structures are thus covered by the images with the narrowest smoothing radii, while the cut-out regions around the sources are filled by values from the images smoothed with a broad Gaussian kernel. The new default values of the implementation of this method in `esplinemap` have been chosen empirically as a brightness level of 5×10^{-4} cts arcsec^{-2} s^{-1} to cut out sources, a minimum smoothing radius of $\sigma = 10$ px, corresponding to 40″ when using standard image binning, and an optimum signal-to-noise ratio of 30. For the catalogue images, these values result in a reasonable compromise between minimising the remaining photon noise in the background image and retaining the resolution for true spatial background variations.

The smoothed background maps are generally in good agreement with the input images. For the 26 835 catalogue images, the median deviation between the total counts of the cheesed background maps and the total counts of the cheesed images is below 2 %. Figure 2 provides an example comparing the spline-fit background and the results of adaptive smoothing for a single observation of the region of η Carinae. The large-scale variation of its complex background structure (Fig. 2a) is well described by the spline fit (Fig. 2b), while small-scale structure becomes additionally visible in the adaptive smoothing fit (Fig. 2c). The differences between the two methods are most obvious in a comparison of the ratios between the original cheesed image (Fig. 2e) and the cheesed background maps (Fig. 2f and g) and in a direct comparison of the background maps (Fig. 2h). Figure 2i shows six of the eight layers with increasing smoothing radii, from which the smoothed background map has been constructed, and Fig. 2d the layer chosen for each image pixel. Visual inspection of selected fields with complex background and of large images processed with both methods confirm a more robust approximation of the observed background by the adaptive smoothing technique in these cases. In images of extended targets that result in large cut-out areas of the cheesed images, spline fits might be preferable. Adaptive smoothing has been chosen as the standard approach for the new catalogue, whose first version is restricted to fields without large extended emission (see Sect. 3).

2.3. Source detection on stacked images

All data products described in Sect. 2.1 are used in parallel by the source-detection tasks, coupling images, exposure maps, and background maps for each observation, instrument, and energy band, and detection masks for each observation and instrument. Simultaneous source detection is performed on them by means of the usual two-step process used for XMM-Newton data (see Paper V): sliding-box source detection followed by maximum-likelihood fitting. All quantities named "likelihood" throughout this process are negative logarithms of probabilities of the null hypothesis that all counts detected arise from random background fluctuations and no source is present.

First, the images are searched for tentative sources by sliding-box source detection using the task `eboxdetect`. The initial run is made with a 20″ box size. Two subsequent runs each increase the box size by a factor two to facilitate searches for extended sources. Detections from previous runs are overwritten if they are found at the same position with a higher signal-to-noise ratio. For each image, a logarithmic likelihood

$$L_i(c_i, c_b) = -\ln \Gamma(c_i, c_b) \quad (1)$$

is calculated that the measured counts c_i within the detection box exceeds the level of pure Poissonian background noise. $c_i =$

$c_s + c_b$ is the sum of source counts c_s and background counts c_b in the detection region in image i. The detection likelihoods of a source in n individual images are summed and converted to a detection likelihood equivalent to that of a detection run on a single image:

$$\mathrm{DET\_ML}_{\mathrm{eboxdetect}} = -\ln\left(1 - \Gamma(n, \sum_{i=1}^{n} L_i)\right) \quad (2)$$

using the regularised incomplete gamma function

$$\Gamma(a, x) = \frac{\int_0^x e^{-t} t^{a-1} dt}{\int_0^\infty e^{-t} t^{a-1} dt}. \quad (3)$$

All images are considered for which the source position lies within the detection mask. Their number can thus vary from source to source within the same detection run. Sources are selected if their equivalent likelihood is higher than a pre-defined minimum, and passed to the task `emldetect` to calculate their parameters by maximum-likelihood fitting. A good likelihood cut represents a compromise between being as complete as possible with respect to real sources and as strict as possible with respect to spurious detections.

The equivalent likelihood depends on the number of photons in the detection box and on the number of images over which they are distributed, because the large number of images in multiple observations leads to large corrections when converting their individual detection likelihoods into the mathematical equivalent of a single-image detection according to Eq. 2. In particular, the sensitivity of the sliding-box detection decreases if few counts are distributed over an increasing number of images (cf. Sect. 2.4). The standard procedure used for single observations has thus been modified for source detection on multiple observations. To avoid the loss of real sources solely because of the number of images, the box detection step on all images was reduced to the same number as used for a single observation: one image for each EPIC instrument and energy band. Therefore, the corresponding images of all contributing observations are combined by the task `emosaic` within `edetect_stack`; likewise the corresponding exposure maps, background maps, and detection masks. These mosaics are only used in the sliding-box run. However, transient sources that are significant in a subset of the observations may disappear from the pre-selection if box detection is limited to the mosaicked images. Hence, `eboxdetect` is additionally run for each individual observation separately. A likelihood cut of five is used in all detection runs. The `eboxdetect` source lists of all observations and the one based on the mosaicked images are merged by the task `srcmatch` within a fixed source-matching radius of $2\sqrt{2}$ times the pixel size, chosen to cover the area of two by two pixels. The matching radius for standard images with a default binning of $4''$ thus becomes $11.3''$. The likelihood column of the merged source list holds the maximum detection likelihood of a source.

Second, the task `emldetect` determines the parameters of all sources in the combined box-detection source list in all images per observation, instrument, and energy band simultaneously by means of maximum-likelihood fitting. Details on the approach are given in Sect. 4.4.3 of Paper V. All input images are combined with their respective background image, exposure map, and detection mask. In each image, the appropriate point spread function (PSF) is chosen at the tentative source position for the instrument configuration. The common source position and extent and the counts per image are fitted within sub-images of $1' \times 1'$ of all input images for which the point spread function overlaps with the field of view as defined via the detection mask. `emldetect` scales each PSF with the measured counts in the individual image. Thus, it does not need to merge PSFs a priori and to make assumptions about the source spectrum. The detection sensitivity is then approximately the same for all incident source spectra (cf. Stewart 2009) and nearly independent of the accuracy of the instrument cross-calibration. To choose the sources that are considered real and to minimise the spurious source content, a significance level needs to be defined. For each source, the detection likelihood in the given fitting setup is derived using the best-fit C-statistic (Cash 1976, 1979), minimising the deviation

$$C_i(c_i) = 2 \sum_{k=1}^{N} (m_k - c_k \ln(m_k)) \quad (4)$$

between measured counts c and the model prediction m in a region of N pixels, where c_i stands for the sum of source counts c_s and background counts c_b in the detection region as before. It is compared to the null hypothesis that the signal purely arises from background counts c_b, and the logarithmic likelihood ratios $L_i = C_i(c_i) - C_i(c_b)$ of the n images involved are combined into the mathematical equivalent of a two-parameter fit as

$$\mathrm{DET\_ML}_{\mathrm{emldetect}} = -ln\left(1 - \Gamma(\frac{\nu}{2}, \sum_{i=1}^{n} \frac{L_i}{2})\right), \quad (5)$$

using the regularised incomplete gamma function Γ (Eq. 3). The ν free parameters are the coordinates of the source, its extent, and the counts per image in which the source lies within the instrumental detection mask. If the likelihood of the source being extended falls below a pre-defined threshold of four or its extent radius below $6''$, the source extent is set to zero and ν is reduced by one to n+2. Using this definition, the degradation of the detection sensitivity with the number of images for faint sources is less prominent than for the likelihood definition of `eboxdetect` (cf. Sect. 2.4), and `emldetect` can be run on all images of the stack simultaneously. Deviating from the standard procedure for individual observations, `emldetect` is called by `edetect_stack` with a minimum detection likelihood of zero in order to store the parameters of each box-detection source and each input image in an intermediate source list without (de-)selecting sources.

A separate module of the task `edetect_stack` is dedicated to the calculation of the final source parameters, the quality assessment, and source filtering. In particular, the total equivalent likelihood over all observations and the likelihood for each individual observation are calculated for each detection and used for source selection. Sources are included in the final source list if at least one of these equivalent likelihoods exceeds a user-defined minimum detection likelihood. As in the 3XMM catalogues, a minimum likelihood of six is required in the stacked catalogue. Example detection images of stacked source detection on archival observations of the Magellanic Bridge region are shown in Fig. 3. For comparison, `emldetect` has also been run for each of the input observations separately, using subsets of the images and maps created for stacked source detection. The resulting detections of all observations are joined within a matching radius of $15''$ and shown as orange boxes and diamonds in the figure. More information on the comparison between source detection on stacks and on single observations follows in Sect. 4.3.

The results of `edetect_stack` are provided in two FITS-format source lists with different structure: one `emldetect`-like list and one in catalogue-like format. The first "classical" one is described in the task documentation[5]. The second new one

[5] `http://xmm-tools.cosmos.esa.int/external/sas/current/doc/emldetect/`

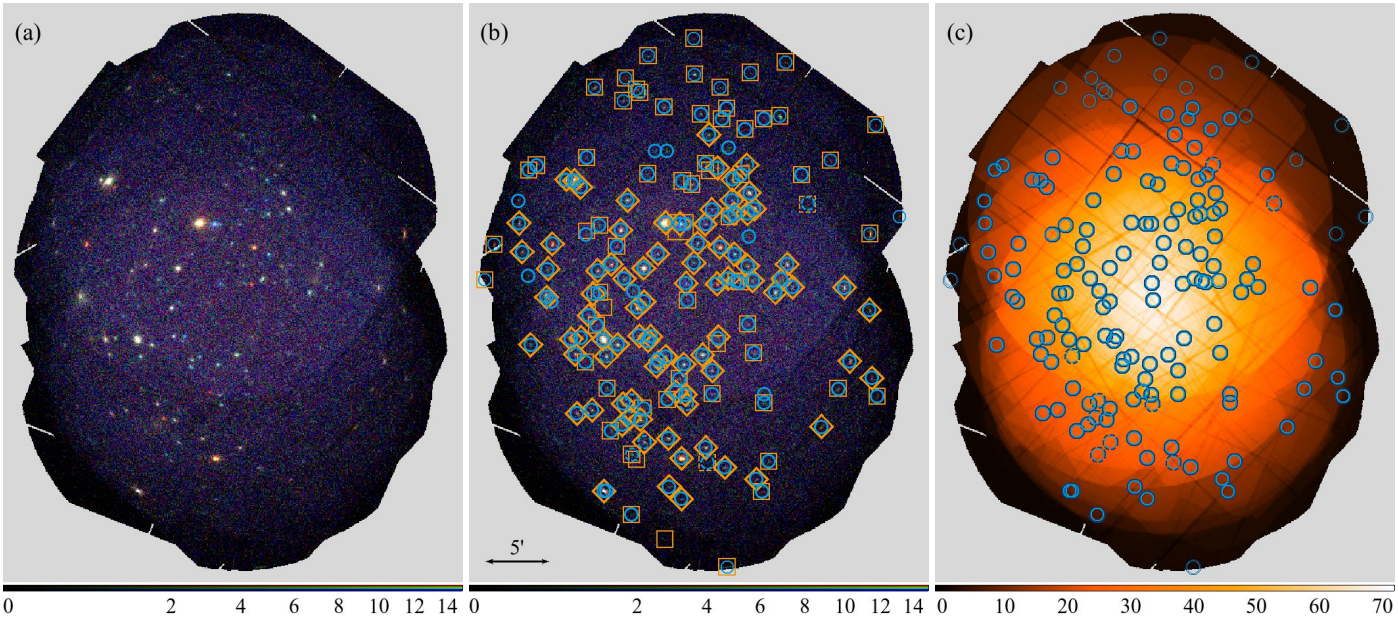

Fig. 3. Example of stacked source detection: six overlapping observations within the Magellanic Bridge. *(a)* Mosaic of all images. The three colour-coded energy bands are: 0.2−1.0 keV (red), 1.0−2.0 keV (green), 2.0−12.0 keV (blue). *(b)* The same mosaic image with source identifications overlaid. *Blue circles:* 158 sources detected by stacked source detection. *Orange boxes and diamonds:* 152 sources detected in the individual observations. Boxes mark sources that are detected in only one contributing observation, dashed symbols mark sources that have been flagged by the task `dpssflag` (cf. Sect. 4.1). *(c)* Mosaic of the vignetted exposure maps with the identifications of the sources in the stacked catalogue. The exposure time has been averaged over the instruments and energy bands and is given in units of kiloseconds in the colour bar.

includes an all-observation all-EPIC summary row for each detected source plus one row for each individual observation for which the source is within the detection mask, giving the source parameters directly derived from the images of the respective observation within the combined fit. The catalogue-like source lists are the basis of the new stacked catalogue. Details on their columns are found in Sect. 4.1 and Table B.2.

2.4. Testing detection efficiency and sensitivity with artificial stacks

The efficiency of the new stacked source detection is investigated in several test runs. Since repeated observations are subject to effects of time-dependent calibration and source variability, long archival observations are used for testing purposes. We create artificial repeated exposures by dividing their event lists into shorter ones and perform source detection on their stacks.

With the first experiment, we investigate the detection efficiency and its dependence on the number of overlapping observations and their exposure time. Selected observations with an exposure time of at least 100 ks are split into two to six nearly equally long sub-exposures. The results of stacked source detection on their combinations are compared to those of source detection on the full observation. Figure 4 shows the number of detections for the observation with identifier 0555780201, which covers the Chandra Deep Field South, and the stacks of its artificial sub-exposures. In the sliding-box detection step, the number of tentative detections with a total equivalent likelihood of at least five decreases drastically if all input images are used in parallel, but remains approximately stable for box detection on mosaicked images (described in Sect. 2.3). A slight increase in mosaic box detections with the number of sub-exposures indicates more false positives. In the maximum-likelihood detection step, the number of reliably detected sources and the sensitivity to low-flux sources also decrease with an increasing number of shorter sub-exposures, because the source counts are distributed across more images, resulting in lower detection likelihoods per image, and the fit has more degrees of freedom, resulting in larger corrections when calculating the total equivalent likelihood. The effect is illustrated in Fig. 5, for simplicity based on the likelihood definition used in `eboxdetect` (Eqs. 1 and 2) for c_s source and c_b background counts in the detection region. If the $c = c_s + c_b$ counts are equally distributed over the images – an unphysical assumption if images are taken in different energy bands –, the likelihood sum is simplified to $n \times L_i(c/n, c_b/n)$. For different image numbers n, the source counts c_s among the c total counts are derived that are needed to detect the source with a total detection likelihood of six in the stack of all n images. Figure 5 shows the detection likelihood that the source with the same count numbers c_s and c_b would have in the fifteen images of a single observation with three instruments and five energy bands. For non-variable sources, for which the measured counts are proportional to the exposure time, this means: The fewer observations are used to cover the exposure time, the higher the detection likelihood; the more observations are used, the more faint detections are lost compared to a single observation over the full exposure time.

With the second experiment, we investigate the detection efficiency for combinations of two observations with different exposure times. 54 long observations in full-frame mode with all three instruments in operation, at least 99 % usable chip area (OBS_CLASS≤2 in 3XMM-DR7), and an exposure time above 70 ks are divided into two parts to construct artificial stacks. The longer exposure has a fixed length, while the shorter one is increased in uniform time steps. Four setups are chosen. The first combines a long sub-exposure that covers 50 % of the total effective exposure time and a short sub-exposure that covers 5 %, 10 %, 15 %, ... of it. The second combines a 65 % exposure and multiples of 2.5 % exposure time. The third combines an 80 % exposure and multiples of 2 %, and the fourth combines a 90 %

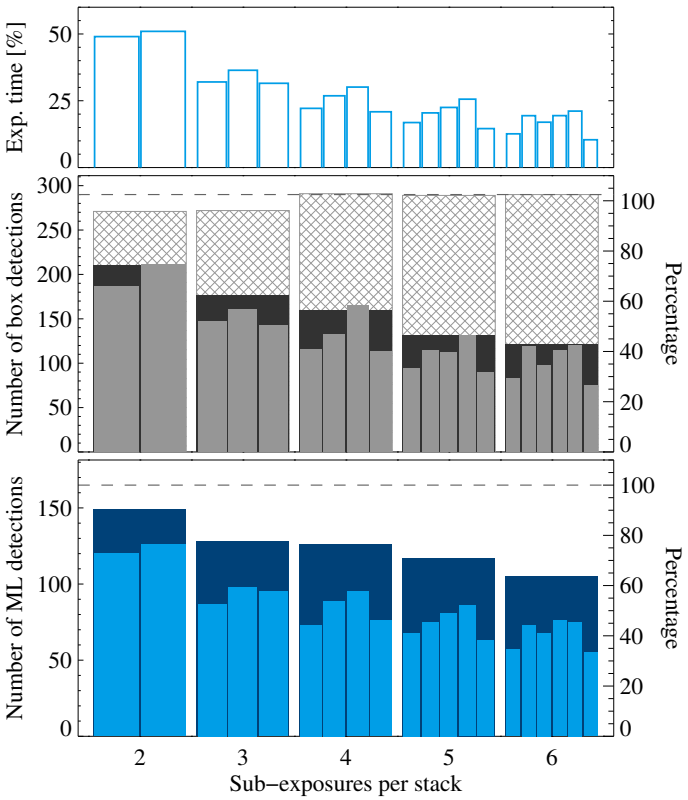

Fig. 4. Stacked source detection on an observation split into several nearly equally long sub-exposures. *Upper panel:* Percentage of exposure time. *Middle panel:* Sliding box detections that are submitted to `emldetect`. Shaded bars mark the sliding-box detections in the fifteen mosaics of all sub-exposures, dark filled bars the detections found when running `eboxdetect` on all individual images simultaneously, and light filled bars the box detections in each individual sub-exposure. *Lower panel:* Final maximum-likelihood detections with a minimum total detection likelihood of at least six in the stack (dark blue) and in the individual sub-exposures (light blue). The dashed horizontal line marks the result of source detection on the full, un-split observation.

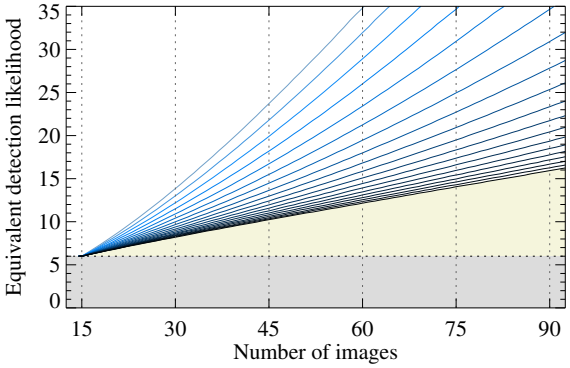

Fig. 5. Detection sensitivity for different numbers of images involved in the fit and different counts, using the likelihood definition of `eboxdetect` for equally long exposed images. The plot shows the detection likelihood that a source would have in a single long observation of duration $T_{\rm exp}$ if it is detected with a total detection likelihood of six in n short observations of duration $T_{\rm exp}/n$. One observation with three instruments and five energy bands comprises fifteen images, marked by dotted vertical lines. A minimum detection likelihood of six is required to detect a source (dotted horizontal line). Each line represents a fixed count number, with counts increasing from top to bottom in the range between 15 and 5 000 in 18 steps of 0.14 dex.

exposure and multiples of 1 % exposure time. For the resulting more than 1 800 combinations of a long with a short exposure, stacked source detection is run to compare the results to single source detection on the longer sub-exposure alone.

Figure 6 shows detection likelihoods and source parameters depending on the exposure time ratios between short and long sub-exposure (see Table B.2 for the definitions of the stacked source parameters). In general, the detection likelihood and thus the number of sources increase with exposure time, while the statistical errors on the source parameters decrease. For two sub-exposures with an exposure time ratio of at least about 40 %, reliably more and fainter sources are detected in the stacks than in the individual sub-exposures. For lower exposure time ratios, the median detection likelihood and the number of sources above the detection limit decrease for pure statistical reasons, because more degrees of freedom of the fit enter Eq. 5. The limiting exposure time ratio above which the total detection likelihood increases with respect to the single detection depends on the signal-to-noise ratio and on the detection likelihood itself. The dependence can be estimated by the simplified calculation introduced in the last section using the `eboxdetect` definition of detection likelihoods. For a fixed count number in the long observation with 15 images, the equivalent detection likelihood is calculated and compared to the combined likelihood of this long and a short observation. Again, counts are assumed to scale linearly with exposure time and to be equally distributed across the images of an observation. The source counts among the chosen total counts are derived for which the detection likelihood in the long observation equals the likelihood in the stack. The curves displayed in Fig. 7 delineate equal detection likelihoods in the long and in the stack of a long plus a short observation as a function of the exposure time ratio and the assumed number of counts. Sources with a detection likelihood above the limiting curve will be detected with a higher total likelihood in the stack. Sources with likelihoods below the curve have a lower detection likelihood in the stack and are lost if they fall below the 3XMM likelihood threshold of six (dark shaded area). The effect is less prominent for the `emldetect` likelihoods which are based on C statistic but still depend on the number of degrees of freedom in the fit. The simulation confirms the empirical finding that higher detection sensitivity is reached for exposure-time ratios above 0.35−0.60, depending on the count number.

The stacked catalogue includes thus all sources which reach the minimum detection likelihood in at least one observation (dark blue dots in the uppermost panel of Fig. 6). This approach preserves strongly variable sources. It is possible, anyhow, that some of the additional sources with total detection likelihood below the threshold of six are spurious. A simple filtering expression on the source list may be applied to extract sources with total detection likelihood above six only.

3. Field selection for the catalogue

The catalogue of sources in overlapping observations is based on data used to compile 3XMM-DR7 and their selection criteria: Per observation, each exposure by an EPIC instrument enters the catalogues if it has a minimum net exposure time of 1 ks, which is the sum of good-time intervals after filtering the event lists, and non-empty images in all five energy bands. This first release of a stacked catalogue comprises good-quality observations which are selected if they fulfil the following five selection criteria (numbers in brackets give the number of the 9 710 3XMM-DR7 observations remaining after each filtering step).

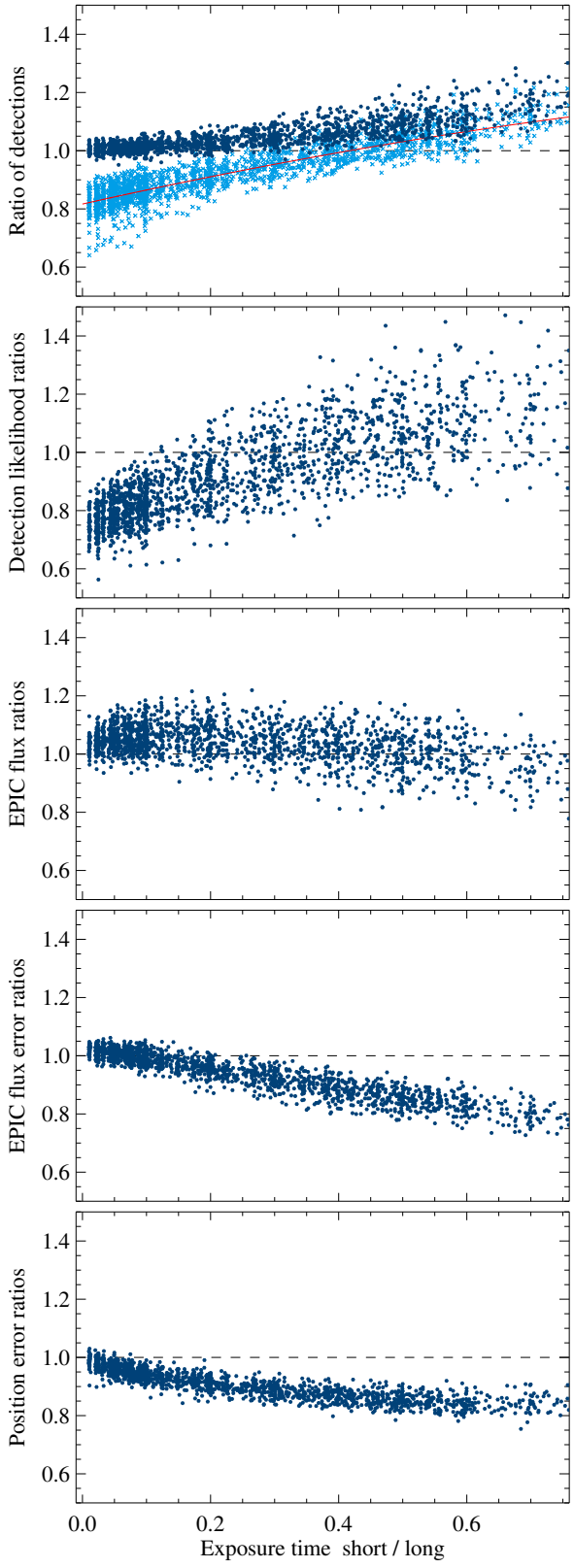

Fig. 6. Source parameters derived from stacked source detection on a longer and a shorter part of long observations, compared to source detection on the longer part only. Each dot represents the ratio of the median values of the sources detected in one stack to the median values of the sources detected in the long sub-exposure alone. Sources with an equivalent detection likelihood above six in at least one sub-exposure are included in the stacked source list. The light blue crosses in the uppermost panel mark the ratio of sources with a total detection likelihood above six only, the red curve a 2nd-degree polynomial fit to them.

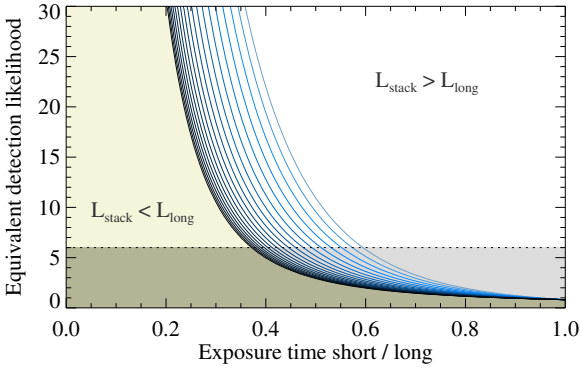

Fig. 7. Numerically calculated limiting detection likelihood in stacks of a long and a short observation for different counts and exposure time ratios, addressing the question of which detection likelihood L_{long} should a source with a certain number of counts (source plus background) have in the long observation to be recovered in the stack of this observation and a short observation with at least the same detection likelihood $L_{stack} = L_{long}$. Sources whose likelihood in the long observation lies above the curve have a higher detection likelihood in the stack. Sources below the curve have a lower likelihood in the stack. The lines represent the same count numbers as in Fig. 5. Counts increase from right to left.

1. All three EPIC instruments were active *(8 022)* and
2. each EPIC instrument was operated in full-frame mode, including Extended Full-Frame Mode for EPIC-pn *(6 937)*.
3. At least 99 % of the chip area are usable according to a classification of OBS_CLASS≤ 2 in 3XMM-DR7 *(4 741)*.
4. The mean background level of each instrument (pn: quadrant) lies below the threshold defined in Sect. 3.1 *(4 370)*.
5. The observation overlaps with another one by at least 20 % in area, approximated as an angular separation of up to 20′ between the aim points *(2 207)*.

OBS_CLASSes indicate the fraction of the usable chip area and are adopted from 3XMM-DR7 without further revision. The assignment of an OBS_CLASS depends on a combination of automatic flagging, manual flagging, and background properties within a partly subjective screening process. By using a maximum OBS_CLASS of 2, we are aiming at excluding complex background structures and large extended objects, which are not the main interest of serendipitous source detection. The fractional area may be slightly different for similar observations of the same field, possibly resulting in different OBS_CLASSes.

Following the selection criteria given above, all suitable observations are sorted into stacks of overlapping observations. Since a minimum overlap of 20 % in area is required, observations belonging to different stacks can still overlap by a smaller amount. To achieve a catalogue of unique sources with maximum total exposure time per source and without duplicate detections in different stacks, a second matching step is imposed on all selected observations. They are re-correlated within a larger radius of 13.5′, equivalent to a maximum separation of 27′ between the aim points of two neighbouring observations. The radius has been determined empirically for this sample of observations: large enough to associate all overlapping areas and small enough not to associate non-overlapping observations.

The resulting list of stacks includes three well-studied survey fields that cannot simply be supplied to `edetect_stack` as a black box, namely M31 and the extra-galactic surveys XXL North and South. Numerous source candidates in the bright core of M31 and the large extent of the XXL surveys prevent them from being processed within a reasonable runtime on standard

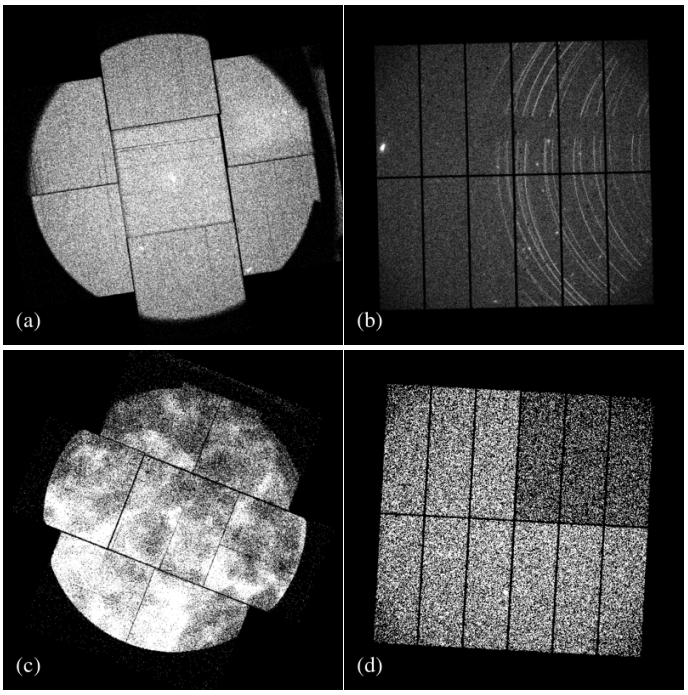

Fig. 8. Examples of different types of increased background intensity in EPIC observations which have been assigned a Cauchy probability above the limit of 87 % using the new method and do not have a HIGH_BACKGROUND warning flag in 3XMM-DR7: *(a)* continuously high background, exceeded by few sources only (obs. id. 0200171401 EPIC-MOS1), *(b)* single reflection patterns (obs. id. 0604820101 EPIC-pn), *(c)* extended diffuse emission (obs. id. 0650220201 EPIC-MOS2), *(d)* different brightness levels of the EPIC-pn quadrants owing to continuous counting mode (obs. id. 0406752601 EPIC-pn). The images are created with a linear colour brightness scale ranging from zero to 10^{-3} times their exposure time.

PCs, which were employed to compile the catalogue. Observations of the M31 core are thus manually de-selected, and 28 observations of its outer parts remain in the catalogue. The large associations comprising the XXL surveys are composed of more than a hundred members each and are completely discarded from the catalogue. The final sample includes 1 789 observations in 434 stacks, the majority of them having two or three members. The number of observations per stack size is given in Table 1.

3.1. Determining continuously high background

Observations with very high particle-induced background need to be identified before performing source detection for the stacked catalogue since their low signal-to-noise can lower the overall detection likelihoods of sources in the field and cause loss of sources. For the 3rd generation of the Serendipitous Source Catalogues 3XMM, an optimised flare filtering technique has been introduced, described in Sect. 3.2.3 of Paper VII. The count-rate threshold of the background light curve above which time intervals are rejected is automatically determined from its signal-to-noise ratio. This method efficiently excludes intervals of high flaring background which are shorter than the total exposure time, but performs less well if it comes to images with persistently high background or features regarded as part of the background because they are not resolved by source detection, examples of which are given in Fig. 8. We employ a new standardised approach to determine the mean background level of an observation from broad-band background images and use it to identify remaining high background emission after applying the good-time intervals from the 3XMM flare filtering. The method is described in appendix A and applied to all 3XMM-DR7 exposures that were taken in full frame, extended full frame, or large window mode to establish a high-background cut. From their median background rate per unit area, probabilities that an observation is affected by high background features are derived for each instrument. From visual inspection of the images and trial runs of source detection on combinations of high- and low-background fields, we choose a probability threshold of 87 % to exclude observations from the pre-selection for the stacked catalogue (step 4 in Sect. 3), reducing the risk of loss of detections because of background contamination. Using this cut, the majority of the observations flagged by the DR7 screeners are also discarded by the automatic procedure and about 350 additional observations (overlapping or not) are newly defined as affected by high-background, like the examples shown in Fig. 8.

Table 1. Stacks from which the new catalogue is compiled. *(a)* Number of observations per stack. *(b)* Number of stacks.

(a)	*(b)*	*(a)*	*(b)*	*(a)*	*(b)*
2	269	11	2	22	1
3	74	12	3	23	1
4	16	13	1	24	2
5	14	15	2	25	2
6	15	16	1	28	1
7	4	18	2	32	1
8	5	19	4	49	1
9	4	20	1	52	1
10	4	21	2	66	1

4. Catalogue construction and properties

4.1. Organisation of the catalogue

For each of the observation groups described in Sect. 3, stacked source detection is run using the new task `edetect_stack`. The stacked catalogue is constructed from the unique source lists of the 434 stacks and comprises 71 951 sources. It lists the parameters from the combined fit for each source and, in addition, one line for each observation that was involved in this fit. All source parameters are directly derived from the results of the simultaneous fit to all observations in a stack. Values per observation refer to the subset of images taken during this observation. The catalogue can be reduced to the one-source-one-row layout of the 3XMM slim source catalogues using a selection expression on the identifier columns given below, such as N_CONTRIB. Its columns are mostly organised in the style of the 3XMM catalogues with the same definitions of their values wherever applicable and fully listed in Table B.2 of the Appendix. In this section, we describe the most relevant parameters, modifications to the 3XMM column definitions, and newly introduced columns.

Source identifier. The unique source identifier SRCID in the stacked catalogue is a 16-digit number, composed of *(i)* a preceding "3", linking it to the convention of the 3XMM catalogues that the detection identifier of individual detections starts with a "1" and the source identifier of unique matches between them starts with a "2", followed by *(ii)* the lowest OBS_ID of the contributing observations (10 digits), and *(iii)* the identifier within the `emldetect` source list (5 digits), for example 3020624020100030 for the thirtieth detection in a stack with 0206240201 being the lowest identifier of all the observations for

which the detection was in the field of view. The five-digits identifiers are not continuous, because the temporary `emldetect` source list comprises all input detections, and only the significant ones among them are transferred to the final source list.

Analogously to the IAU name of 3XMM sources, each source is attributed an additional identifier SRCNAME of the form "3XMM *hhmmss.s±ddmmss* s", composed of the sexagesimal right ascension and declination of the source and an appended "s", standing for its origin in the stacked catalogue.

Observations included. Column N_OBS gives the total number of observations per stack, column N_CONTRIB the number of contributing observations for which the source position is inside the field of view. Both column values are set to null (undefined) in the observation-specific rows and can thus be used to select the summary rows per source.

Source coordinates. The position of the source is the result of the simultaneous fit and considered to be the same in all contributing observations and images, while the number of source counts are determined separately per image (see Sect. 4.4 for a discussion of the astrometric accuracy). It is given in equatorial, galactic and image coordinate systems in the RA, DEC, LII, BII, and X_IMA, Y_IMA columns, respectively. Image coordinates refer to the common coordinate system of each stack (see Sect. 2.3) and are listed together with their individual errors. The combined position error RADEC_ERR is calculated from the errors on the image coordinates as $(\sigma^2_{\mathrm{X\_IMA}} + \sigma^2_{\mathrm{Y\_IMA}})^{0.5}$, converted to arcseconds. For symmetric errors in both dimensions, RADEC_ERR/$\sqrt{2}$ is the one-dimensional 1σ position error, giving the coordinate interval that includes 68 % of normally distributed data points. $\sqrt{2.3/2}\times$RADEC_ERR is the two-dimensional error, giving the radius of a circularised ellipse that includes 68 % of normally distributed data points.

Equivalent detection likelihoods. Maximum detection likelihoods are determined per input image, summed, and converted from the total number of degrees of freedom to the mathematical equivalent of a two-parameter fit (see Sect. 2.3). The number of degrees of freedom is two for point sources and three for extended sources plus the number of images involved in the fit (equalling the number of instruments in each observation, for which the mask is valid at the source position, times the number of energy bands) and varies from source to source. The decision whether a detection enters the final source list is based on the equivalent likelihoods. Sections 2 and 4.3 describe how a large number of input images can affect them and thus the source selection in the fitting process. Sources with a minimum equivalent likelihood of six in the whole stack or at least one contributing observation are thus included in the stacked catalogue.

Source flux. The fitted count rate per image is converted to flux using the energy conversion factors (ECFs) of Paper VII. All-EPIC fluxes are means of the fluxes per instrument and observation weighted by their inverse squared errors. They are null with undefined flux errors but non-zero count errors for an observation if no counts are found within the PSF area of a source. The ECFs depend on the instrument, the observing mode, and the filter used, and on the spectral shape of the source. Therefore, the combined fluxes merging different instruments and merging different instrumental setups across the observations are affected by cross-calibration uncertainties as described by Mateos et al. (2009). The underlying spectral model of the 3XMM ECFs is an absorbed power law with a column density of 3×10^{20} cm^{-2} and a photon index of 1.7.

Source extent. The radial extent of a source, given in arcseconds, and its extent likelihood are fitted simultaneously in all observations. The β model used to parameterise the source extent is described in Sect. 4.4.4 of Paper V. Sources with an extent below 6″ or an extent likelihood below 4 cannot be resolved and are considered point-like. Their source extent is set to zero and their extent likelihood to null.

Mask fraction. The PSF-weighted detector coverage of a source is given for each instrument separately. During an observation, it is conservatively defined as the minimum mask fraction of the five energy bands, indicating the most restrictive mask. The stacked mask fraction is the largest mask fraction of the contributing observations, indicating the best observation.

Source flags. A modified version of `dpssflag`, the task also in use for the 3XMM catalogues, is employed for an automated quality flagging to warn the user about complexities in the environment of the source that might affect the significance of the detection or the source parameters and their accuracy. The sources are not visually screened. Strings of nine booleans indicate different potential issues of a detection in total and for each instrument, described in detail in Sect. 7.3 of Paper V. A true EPIC flag means a warning for at least one instrument. The nine booleans are converted to a single integer summary flag STACK_FLAG. Sources with a flag value of "0" come without any warning. Flag "1" indicates reduced detection quality in at least one instrument and observation: low detector coverage or a source position close to another source or to bad detector pixels. The list of known bad pixels is hard-coded within the task `dpssflag`. "2" is attributed to potentially spurious sources, for example those found within the PSF radius of another source. A flag value of "3" in the summary row indicates that the source has received flag 2 in all contributing observations. The integer flags are not directly comparable to the integer SUM_FLAG in the other 3XMM catalogues, which have been set for individual observations and include additional information from visual screening.

Long-term variability between observations. Three new sets of parameters provide information on the inter-observation variability of a source: *(i)* the χ^2 of the long-term variability and the associated probability that the flux measurements are consistent with those of a non-variable object, *(ii)* the absolute ratio between maximum and minimum flux with its 1σ-error, and *(iii)* the maximum flux variation in terms of sigma. Each of them is directly derived from the EPIC fluxes and flux errors in all contributing observations and in each of the five energy bands separately, resulting in six columns per quantity.

$$\mathrm{VAR\_CHI2} = \frac{1}{n-1}\sum_{k=1}^{n}\left(\frac{F_k - F_{\mathrm{EPIC}}}{\sigma_k}\right)^2 \tag{6}$$

is a reduced χ^2 of flux variability between the mean all-EPIC flux F_{EPIC} over all observations and the individual fluxes F_k derived for each observation, k running from 1 to number n of observations. The associated VAR_PROB describes the probability that the observed flux values are consistent with constant source flux over all observations. It is the cumulative chi-square probability

$$\mathrm{VAR\_PROB} = \int_{\chi^2}^{\infty} \frac{x^{\nu/2-1}e^{-x/2}}{2^{\nu/2}\Gamma(\nu/2)}dx \tag{7}$$

to reach at least VAR_CHI2=χ^2 at $\nu = n-1$ degrees of freedom. A low value of VAR_PROB thus indicates a high chance that the source shows inter-observation flux variability.

$$\mathrm{FRATIO} = F_{\max}/F_{\min} \tag{8}$$

gives the ratio between the highest and the lowest flux recorded across the observations, and

$$\mathrm{FRATIO\_ERR} = \left(\frac{\sigma^2_{F\min}}{F^2_{\min}} + \frac{\sigma^2_{F\max}}{F^2_{\max}}\right)^{0.5}\frac{F_{\max}}{F_{\min}} \tag{9}$$

its 1σ error.

$$\mathrm{FLUXVAR} = \max_{k,l\in[1,n]} \frac{|F_k - F_l|}{\sqrt{\sigma_k^2 + \sigma_l^2}} \quad (10)$$

is the largest difference between pairs of fluxes in terms of sigma, with k and l running from 1 to number n of observations.

Observation characteristics. Each row per observation includes the modified Julian dates of its start and end time. In the summary row per source, the MJDs of the beginning of the first and the end of the last contributing observation are given. Filter, instrument submode, and mean position angle of the spacecraft are listed for each observation.

Columns copied from 3XMM-DR7. For sources with a counterpart in the 3XMM-DR7 catalogue of sources, information on position, quality flag, and intra-observation variability of the 3XMM-DR7 source are copied to the summary rows of the stacked catalogue. The observation-specific rows list the parameters of the 3XMM-DR7 detection that contributes to the unique source, if one is found. Column DIST_3XMMDR7 gives the distance between the stacked detection and the 3XMM-DR7 counterpart. More details on the matching can be found in Sect. 4.6.

4.2. General characteristics

The 71 951 unique sources in the stacked catalogue are detected in 1 789 observations in 434 stacks, covering more than sixteen years of observations in total. The longest time span between the beginning of the first observation and the end of the latest observation of a source is 14.5 years. 96.6 % of the sources have been assigned a good automatic quality flag of 0 or 1, and 74.3 % are detected with a total likelihood of at least 10; a somewhat smaller share than in the 3XMM-DR7 catalogue of unique sources (80 %), where the combined detection likelihood of repeatedly observed sources is given as the highest per-observation likelihood, while the total likelihood in the stacked catalogue is calculated using Eq. 5. 57 665 of the sources are covered by more than one observation with a maximum of 23 visits of a source. An overview of the catalogue properties is given in Table 2. Since most of the stacks comprise two observations, the majority of sources has been detected twice (Fig. 9). The absolute number of catalogue sources and covered sky area decrease with increasing stack size because few large stacks are included in the catalogue. The relative source density per unit sky area increases with the stack size thanks to the long total exposure.

With the longer effective exposure time, given per source in the ONTIME catalogue columns, more counts are collected. Hence, the sources are measured with higher detection likelihoods, and extended sources additionally with higher extent likelihood, shown in Fig. 10. In its left panels, the effect of the new likelihood cut used for the stacked catalogue becomes obvious. While a hard cut of six has been applied to the other 3XMM catalogues, sources with a total equivalent detection likelihood below six are present in the stacked catalogue: They exceed the threshold in at least one contributing observation, not in the whole stack. A hard cut of four is applied to the extent likelihood, simultaneously determined from all contributing observations, as in the 3XMM catalogues. Figures 10–15 include the almost 20 % of catalogue sources from non-overlapping chip areas with one contributing observation.

Owing to the larger exposure time and count number of the stacked observations, stacked source detection becomes more sensitive to faint sources, and the flux errors decrease significantly with exposure time, confirmed by the increasing number of catalogue sources having low flux and small flux errors with increasing EP_ONTIME (Fig. 11). The higher parameter accuracy at long exposure times, shown on the example of the flux errors in the right panel of Fig. 11, applies to all error columns in the catalogue. The smaller errors reflect the smaller scatter of possible parameter values and higher fit accuracy in the stacked source detection. XMM-Newton source detection employs the C statistic in the maximum-likelihood analysis, which is distributed as χ^2 plus an additive term proportional to $n^{-0.5}$ (Cash 1976, 1979), negligible for large count numbers n. The one-dimensional 1σ error on a parameter is derived by stepping the parameter until $C = C_{\mathrm{min}} + 1$ is reached, corresponding to the 68 % accuracy level of a χ^2 statistic. The confidence limits of parameters derived from images with few photons in the source-fitting area and of highly coupled parameters may be actually larger than the ones derived for $C = C_{\mathrm{min}} + 1$, and an additional error component might thus be considered when interpreting the statistical errors on the stacked parameters, for instance regarding fluxes of sources close to the detection limit or position matches in a cross-correlation with other catalogues. For the position error, an estimate is derived in Sect. 4.4.

The distribution of source fluxes in the stacked catalogue – in total and per energy band – is shown in Fig. 12. It is similar to the

Table 2. Overview of the catalogue of unique sources in spatially overlapping XMM-Newton observations, selected from the 3XMM-DR7 observations taken between 2000 February 3 and 2016 December 15.

Description	Number
Number of stacks	434
Number of observations	1 789
Time span first to last observation	Feb 20, 2000 – Apr 02, 2016
Approximate sky coverage	150 sq. deg.
Approximate multiply observed sky area	100 sq. deg.
Total number of sources	71 951
Sources with several contributing observations	57 665
Sources with flag 0 or 1	69 526
Total detection likelihood of at least 10	53 492
Extended sources (radius $\geq 6''$)	3 346
Point sources with VAR_PROB$\leq$1 %	5 607
Point sources with VAR_PROB$\leq 10^{-5}$	1 927

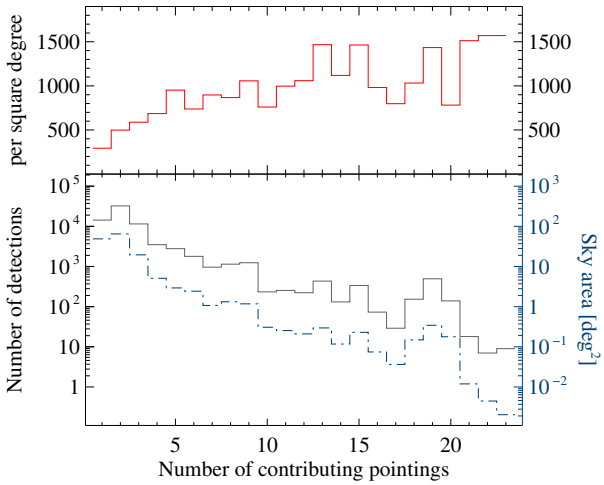

Fig. 9. Number of detections (grey solid), detections per square degree (red solid), and approximate sky coverage in square degrees (blue dash-dotted) per number of contributing observations.

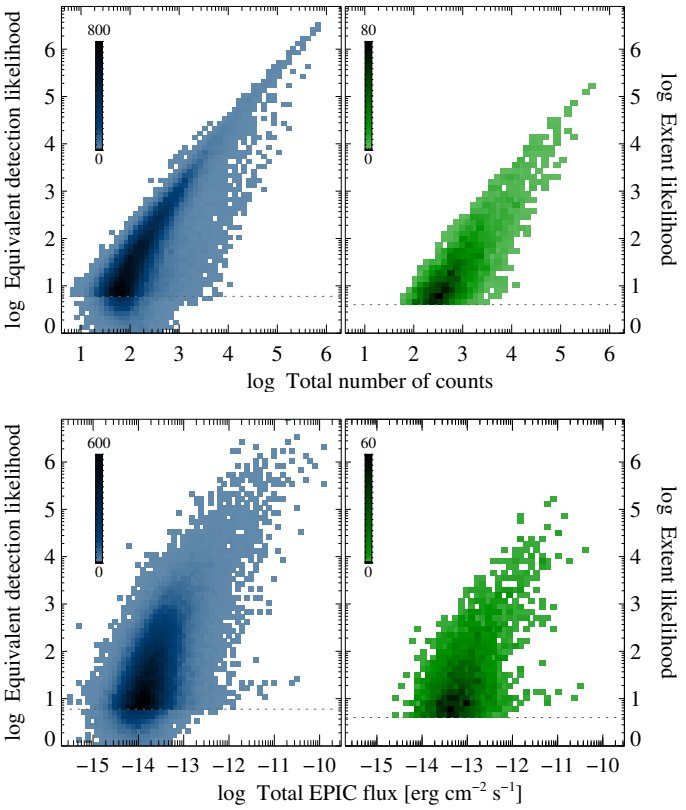

Fig. 10. Relation of detection and extent likelihoods to source flux and counts. Dotted lines mark the lower limits: minimum detection likelihood per observation to include a source in the source list and minimum extent likelihood per fit to consider a source extended. Colour density scales with the source number per plotting bin.

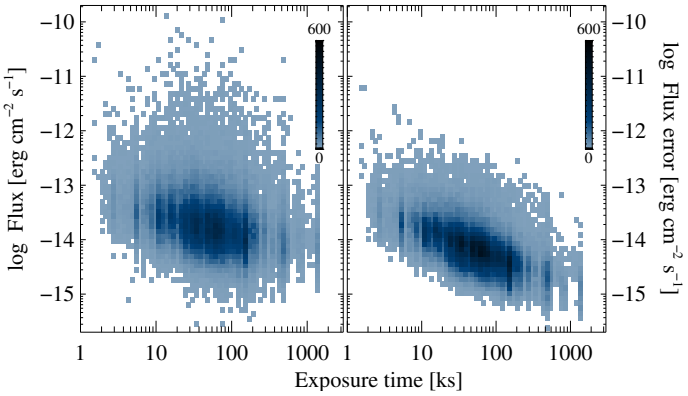

Fig. 11. Relation between exposure time EP_ONTIME and all-EPIC fluxes (left panel) and flux errors (right panel). All-EPIC fluxes are the weighted means of all fluxes in the energy bands between 0.2 and 12.0 keV. Colour density scales with the source number per plotting bin.

distributions determined from the other 3XMM catalogues, in agreement with the expectation that the fluxes derived by stacked source detection are consistent with those derived from the individual observations, but better constrained.

Almost 4.7 % of the catalogue sources are resolved as extended with a core radius of the β-profile extent model of at least 6″. In general, the characterisation of extended sources is affected by larger uncertainties than that of point sources: their intensity profile is less sharp, imposing larger position errors on extended sources, and the beta function is only an approximation to the true extent profile, imposing uncertainties on the measured

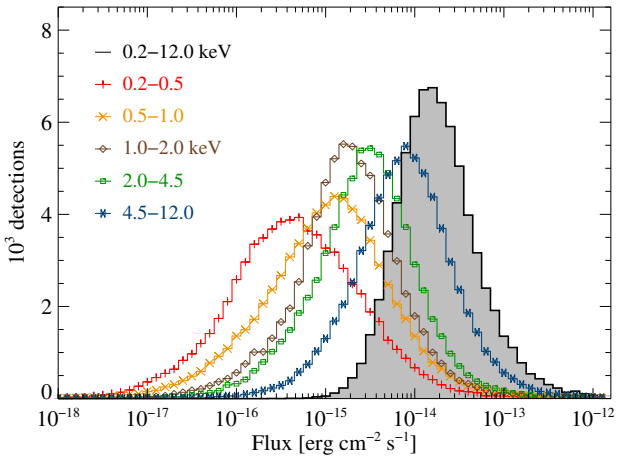

Fig. 12. Flux distribution in the catalogue of sources from overlapping observations, in total (grey, filled) and for each of the five energy bands (energy increases from left to right).

extent radius. For short observations and faint extended sources, the measured extent depends on the exposure time if insufficient counts are collected to describe them reliably. In stacked source detection, the source extent can now be fitted simultaneously in all observations irrespective of their individual exposure time, making use of the total counts. While uncertainties remain, for example owing to deviations from the true extent profile of a source, the extent parameters can be determined more precisely, and the risk of fitting background fluctuations by spurious extended sources is lower. The experiments with artificial stacks, described in Sect. 2.4, actually confirm that extended sources are detected more reliably even if observations of different durations are combined. The high percentage of sources with quality flag 0 or 1 among all extended sources, similar to the one of good detections among the point sources, also indicates reasonably low spurious content. For comparison, 10 % of the unique sources in 3XMM-DR7 have at least one extended contributing detection, irrespective of the quality flag after visual screening. If only those unique 3XMM-DR7 sources are considered to which at least one detection with a good detection flag of 0 or 1 after visual screening contributes, then the fraction of sources comprising an extended detection reduces to 3 %. Still, large position errors and quality flags 2 and 3 in the stacked catalogue should be taken as signs that a detection is uncertain.

4.3. Detection sensitivity and reliability

To quantify the improvement of the detection sensitivity of stacks over individual observations within consistently designed data sets and source-detection runs, source detection has been performed separately on each catalogue observation, using the same detection method and parameters as applied to the stacks of observations. The 126 658 individual detections were matched into a joint list of 71 921 tentative unique sources within a matching radius of 15″. We compare the stacked sources *(i)* with the individual detections and *(ii)* with the joint single-observation detections, again using a matching radius of 15″. The joint source lists are expected to deviate from 3XMM-DR7 due to the different background models and image creation. Section 4.6 includes a comparison with 3XMM-DR7.

Figure 13 shows distributions of four main source parameters of the stacked catalogue and the individual detections, all normalised to their total number. The longer effective ex-

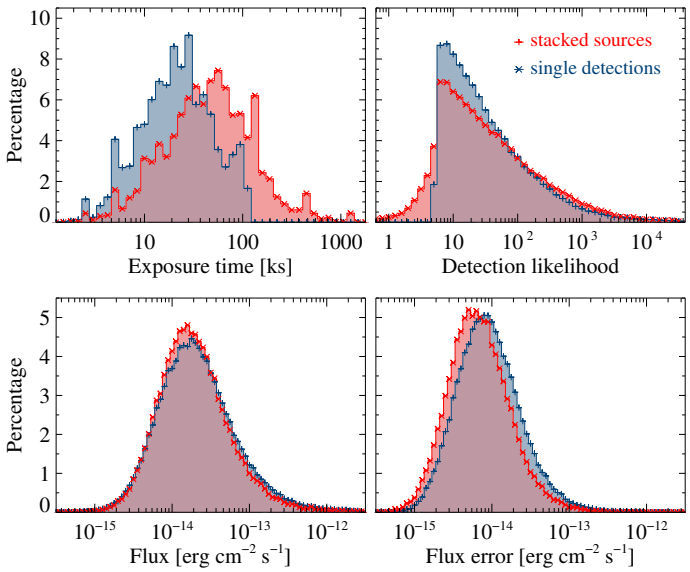

Fig. 13. Normalised distribution of all-EPIC good time intervals, detection likelihoods, fluxes, and flux errors of the sources from stacked source detection (red) and of the individual detections in the source lists per single observation (blue).

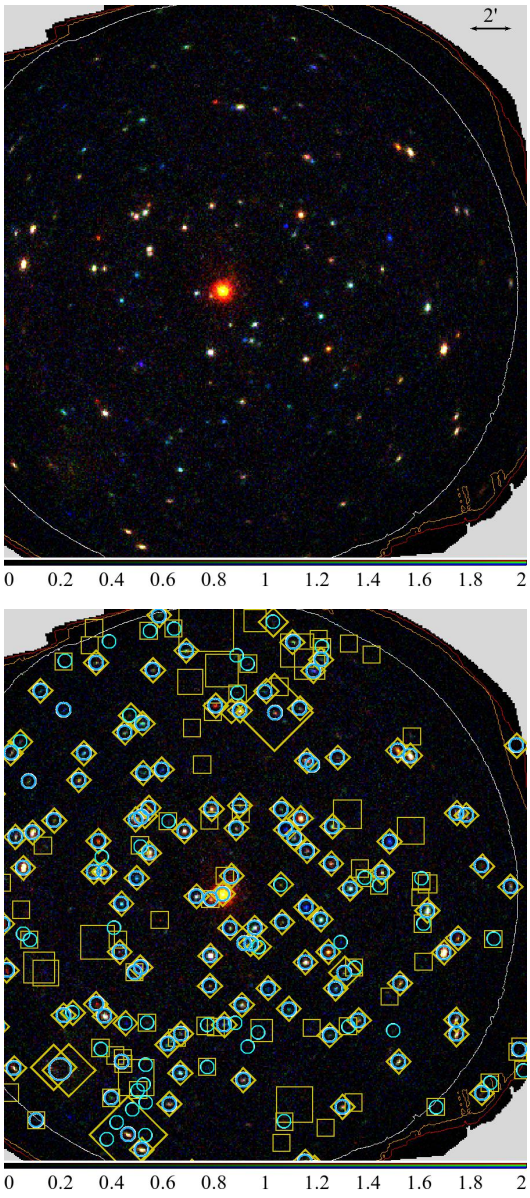

Fig. 14. Example with large deviations between stacked and joint source list: nineteen observations of HD 81809. For clarity, the mosaicked image is shown both without and with source identifications. *Blue circles:* Sources detected in the stack. Thick circles are used for sources with an equivalent detection likelihood above six in more than two observations, thin circles for the others. *Yellow boxes:* Joined individual detections. Thick diamonds are used for those merged from more than two observations, thin squares for the others. The plot symbols have a minimum extent of 40″ and scale with the source extent if it is larger than that. The contours enclose areas within at least two (red), seven (orange), and twelve (white) observations overlap.

posure times and smaller flux errors of the stacked catalogue with respect to all detections from the individual observations are clearly visible. The stacked detection likelihoods tend to be higher than that of the individual detections, but include small values for sources that are significant in only one contributing observation. Fluxes are expected to be consistent. Differences in their distributions may indicate a larger share of low-flux sources in the stacked catalogue and better sensitivity to faint sources.

To quantify potential gain and loss of sources of stacked over individual source detection, the detections in individual observations that are not recovered by stacked source detection are investigated. 4 931 detections are found in the single runs only. The vast majority – over 98 % – are detected in one observation with low likelihood without a potential second detection within 15″, although located in overlap areas. About 10 % may be the subject of source confusion, overlapping with neighbouring detections within a matching radius of 30″. A large fraction of 40 % of the 4 931 not recovered "single-only" detections are extended, 416 even with an extent radius of more than 1′. They have larger positional uncertainties which may affect the positional matching, and a high chance to be spurious detections.

For the match between the stacked catalogue and the joint source lists, the positions of the joined sources are defined as the mean positions of the contributing single detections and their extent as the maximum extent of the single detections. 4 347 sources are found by stacked source detection only, which means: they have no counterpart in the joint source list within a radius of 15″. Most of them are located in areas covered by several observations. Only 15.7 % of them are extended, 121 with an extent radius of more than 1′. The point-like stack-only sources tend to have higher detection likelihoods and slightly better constrained fluxes than point-like single-only detections. This may indicate that a larger fraction of the stack-only than of the single-only sources are reliable detections.

It is worth mentioning that this analysis is based on the modified likelihood cut of the stacked catalogue, including sources with a total detection likelihood below six if they exceed six in one observation. With respect to spurious detections, stacked source detection can still perform better than source detection on single observations in overlapping areas, for instance if the positions of faint sources are poorly constrained in the individual observations and offset from each other. The merging algorithm does not identify them as different incarnations of the same unique source, while stacked source detection uses the combined results of the sliding-box detection runs and starts from the most likely detection. Once a reasonable maximum-likelihood PSF fit is found, the other less likely sliding-box detections within the PSF fitting radius are discarded, and one stacked source with a slightly higher detection likelihood replaces several lower-likelihood detections from the individual source-detection runs.

Figure 14 illustrates the differences between stacked and non-stacked detections in an example stack of 19 observations. The individual images are background-subtracted, normalised by their exposure time per pixel, and combined into a mosaic for display purposes. All joint-only detections have few counts in few contributing observations and may be spurious. Some joint-only detections are very extended and thus most likely also spurious. Some stack-only sources exceed the detection likelihood limit in only one or two contributing observations and might be spurious as well. Visual inspection of all stacked and joint source lists has led to the conclusion that many single-only detections are uncertain, very close to the detection limit, or obviously spurious and that stacked source detection results in a smaller fraction of spurious sources than joining individual detections.

4.4. Astrometry

The source positions in the stacked catalogue are determined simultaneously from all observations using their respective calibration. For the 2XMM and 3XMM catalogues, the individual observations are rectified after performing source detection by comparing the measured X-ray positions of the brightest sources per field with source positions in optical and infra-red catalogues and applying the derived positional shifts and field rotation to all sources in the field. The approach cannot be applied directly to the source lists, from which the stacked catalogue is compiled, because the different observations per stack might be affected by different positional shifts. New, more detailed PSF models, upgrades to the source-detection tasks, and a refined boresight calibration, however, have helped to determine the source positions for the 3XMM catalogues more precisely than for previous versions even without this field rectification (see Paper VII). Using them, no additional astrometric corrections are applied to the first stacked catalogue. The stacked position errors RADEC_ERR are pure statistical errors from the joint fit, giving the uncertainties of the measurements. Systematic uncertainties like the inaccuracies of the (positional) cross-calibration of the contributing observations are thus not included in the stacked catalogue, but can be estimated from the deviations between measured and expected positions of point sources with well-defined astrometry.

For the 2XMM catalogues (Paper V), the mean systematic position error has been determined to be about 1″ before and 0.35″ after astrometric correction from a comparison with optical quasar positions in the Sloan Digital Sky Survey (SDSS), assuming that the error-normalised angular distances are Rayleigh distributed. Following this approach, the (uncorrected) X-ray positions of the unique sources of the stacked catalogue are matched with the latest SDSS release DR12 (Blanton et al. 2017) within a radius of 15″ without further restrictions on off-axis angle or quality flags. The 1 288 quasars among the best matches are selected, and the histogram of their positional offsets $x = \delta/\sigma$ is compared with a Rayleigh distribution $xe^{-0.5x^2}$, δ being the angular distance between the SDSS position and the one in the stacked catalogue, σ the square root of the sum of their squared circularised one-dimensional position errors. An additional error component on the X-ray position is varied until best agreement between the measured histogram and the Rayleigh distribution is reached. Since the nature of the additional component is unknown, the fit is performed for two alternatives, a quadratic sum $\sigma = (\sigma^2_{\rm stat} + \sigma^2_{\rm sys})^{0.5}$ and a pure linear $\sigma = \sigma_{\rm stat} + \sigma_{\rm sys,lin}$. The best fits are achieved with a quadratically added component of $\sigma_{\rm sys}$=0.73″ and with a linearly added component of $\sigma_{\rm sys,lin}$=0.43″, respectively, which can be considered the parameter range of the mean systematic error on the stacked source positions. Figure 15 includes the position offsets between stacked sources and SDSS quasars normalised by the pure statistical errors and with the linearly added 0.43″ uncertainty on the X-ray positions, and the respective Rayleigh distribution.

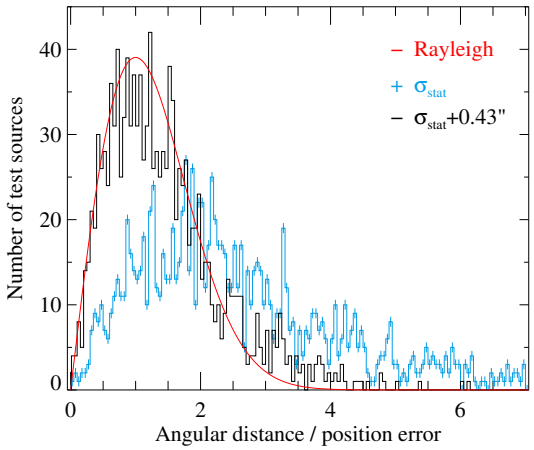

Fig. 15. Error-normalised position offsets between sources in the stacked catalogue and associated quasars in SDSS-DR12 compared to a Rayleigh distribution (red). *Light blue:* Based on the one-dimensional purely statistical position errors RADEC_ERR/$\sqrt{2}$ given in the catalogue. *Black:* Using the best-fit additional error component 0.43″, linearly added to the statistical 1d error on the X-ray position.

For comparison, the same method is applied to the uncorrected positions of the individual detections in 3XMM-DR7. Their distribution of offsets from associated SDSS quasars is fitted with $\sigma_{\rm sys}$=1.01″ and $\sigma_{\rm sys,lin}$=0.59″. In the 3XMM catalogues, the field rectification is used to derive additional information on the position error, and the combined error of the field translation and rotation is applied as additional error component. Its median in 3XMM-DR7, restricted to detections with a quasar association, is 0.43″. Although derived from astrometrically uncorrected data, the parameter range of the additional error component for the stacked catalogue is far below the pixel size and smaller than for the individual 3XMM detections in the same sample of observations.

4.5. Long-term source variability between observations

The stacked catalogue can serve as a database for long-term variability of serendipitous XMM-Newton sources: Irrespective of the detection probability within a single observation, fluxes and flux errors are determined for each observation that covers the source of interest without the need to match individual detections and to determine upper limits of the flux, increasing the chance to identify transients. Inter-observation variability in XMM-Newton data has been explored previously by Lin et al. (2012) based on high signal-to-noise detections in 2XMM-DR3i and through the EXTraS project (Exploring the X-ray Transient and variable Sky, De Luca et al. 2016) based on 3XMM-DR5 and slew observations, published as the EXTraS long-term Variability Catalogue (Rosen & Read 2017).

From the total mean flux and the all-EPIC fluxes per contributing observation of each stacked catalogue source that has been observed at least twice with non-zero counts, five quantities describing its inter-observation variability are derived (introduced in Sect. 4.1). Since they are based on mean fluxes of

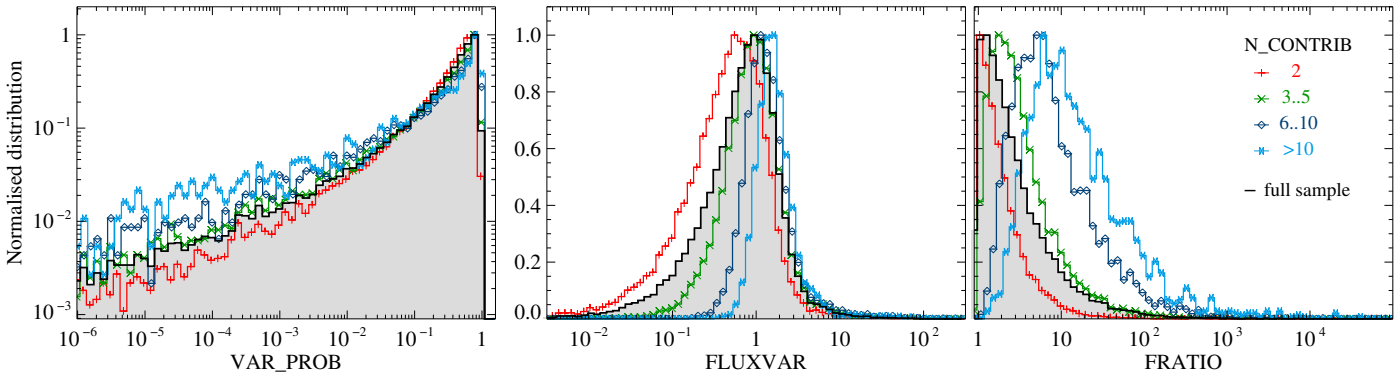

Fig. 16. Three of the all-EPIC long-term variability parameters for point sources and their different dependence on the number of contributing observations. A low value of VAR_PROB and high values of FLUXVAR and FRATIO can indicate a long-term variable source. All histograms are normalised to their maximum for comparison.

the observation-level snapshots, they provide information on potential long-term variability only and are not probed for intra-observation variability. For 787 detections, the source flux during one contributing observation has been set to null, because no counts were detected during this observation. They do not contribute to the variability parameters in the present catalogue. Upper limits for such cases will be included in future releases.

The parameters show little dependence on the energy band, with the highest values being present in the well-populated bands 2 – 4, but clear dependence on the number of contributing observations N_CONTRIB. VAR_PROB is least dependent on N_CONTRIB because it is normalised by the number of degrees of freedom. Distributions of the variability parameters for different N_CONTRIB are given in Fig. 16. All histograms peak at higher parameter values for larger N_CONTRIB. This dependence on the number of involved data points is qualitatively consistent with the results of Rosen & Read (2017). They simulate sparsely sampled long-term light curves for objects with constant mean fluxes, derive the maximum flux variations in terms of sigma, and show their dependence on the number of light-curve points, owing to larger statistical fluctuations for a larger number of points. More than half of the repeatedly observed sources in the stacked catalogue are covered by only two snapshots. Thus, the distributions for low numbers of contributing observations dominate the overall result. Throughout this paper, we use a generous tentative variability limit of VAR_PROB≤1 %. 5 607 or 10.2 % of the point sources in the catalogue with at least two contributing observations may be considered potentially long-term variable according to this criterion. 1 927 or 3.5 % have a probability below 10^{-5}. Users are recommended to carefully choose the variability parameters and limits to define long-term variability depending on their research subject and the type(s) of their objects of interest.

Several effects that are not intrinsic to the source may lead to seemingly large flux variations. Spurious, often extended detections, can appear in some observations, for example on detector features like bad pixels, stray light, or imperfect PSF fits to bright and / or extended sources. Many of them can be identified and removed by applying cuts to the extent parameters and to large errors on the flux ratios. In a few cases, poorly constrained flux values in individual observations can mimic variability. Time-dependent calibrational uncertainties (cf. Read et al. 2014; Plucinsky et al. 2017) may also slightly contribute to apparent source variability. High-proper motion objects are prone to mis-classifications, as they cannot be uniquely identified by the source-detection process which assumes stable source positions in all images. For example, the high proper motion binary 61 Cygni separates into ten individual sources from eighteen overlapping observations in the stacked catalogue, recorded at differently high levels of (apparent) variability.

In the 3XMM catalogues, intra-observation variability is investigated for all detections with at least 100 counts. We select sources with a counterpart in the 3XMM-DR7 catalogue (see Sect. 4.6) and compare the parameters on intra- and inter-observation variability. Some, but not all of them are expected to be identified on all time scales as variable. A long-term variable source may be constant over the time span of a single observation, and variability on short time scales does not necessarily imply long-term variability of the mean fluxes, as for regular periodicity of up to a few hours. Information on short-term variability is provided for 11 472 point-like 3XMM-DR7 counterparts to stacked sources. 620 are flagged as short-term variable in at least one 3XMM-DR7 observation, and 509 of them have several observations in the stacked catalogue. As expected, a considerable number of short-term variable sources also shows signs of long-term variability: 384 with a probability below 1 % that the measurements are consistent with constant flux, 308 with a probability below 10^{-5}. Thus, 125 of the sources, whose 3XMM-DR7 counterpart is flagged as short-term variable, show no clear sign of long-term variability in the stacked catalogue. For 39 of them, the 3XMM-DR7 observation that triggered the short-term variability flag is not part of the sample selected for the stacked catalogue according to the criteria listed in Sect. 3.

To demonstrate the potential of the new variability parameters for transient detection and the advantage of the combined source fitting, we select tentatively variable stacked sources and match them with catalogues from surveys at different energies within a radius of 5″, similar to the multi-wavelength cross-matching presented at the end of Sect. 4.6. We de-select sources with a matching identification in Simbad (Wenger et al. 2000), a counterpart in the pre-release version of the second Chandra Source Catalogue CSC2 (Evans et al. 2010), or a spectral classification in SDSS-DR12 (Blanton et al. 2017). Two example light curves of the remaining candidates for new long-term variable X-ray sources are shown in Fig. 17.

4.6. Cross-matching with the 3XMM serendipitous source catalogue DR7 and multi-wavelength catalogues

Since the stacked catalogue is based on a subset of 3XMM-DR7 observations, its sources have been positionally cross-matched with the 3XMM-DR7 catalogue of unique sources

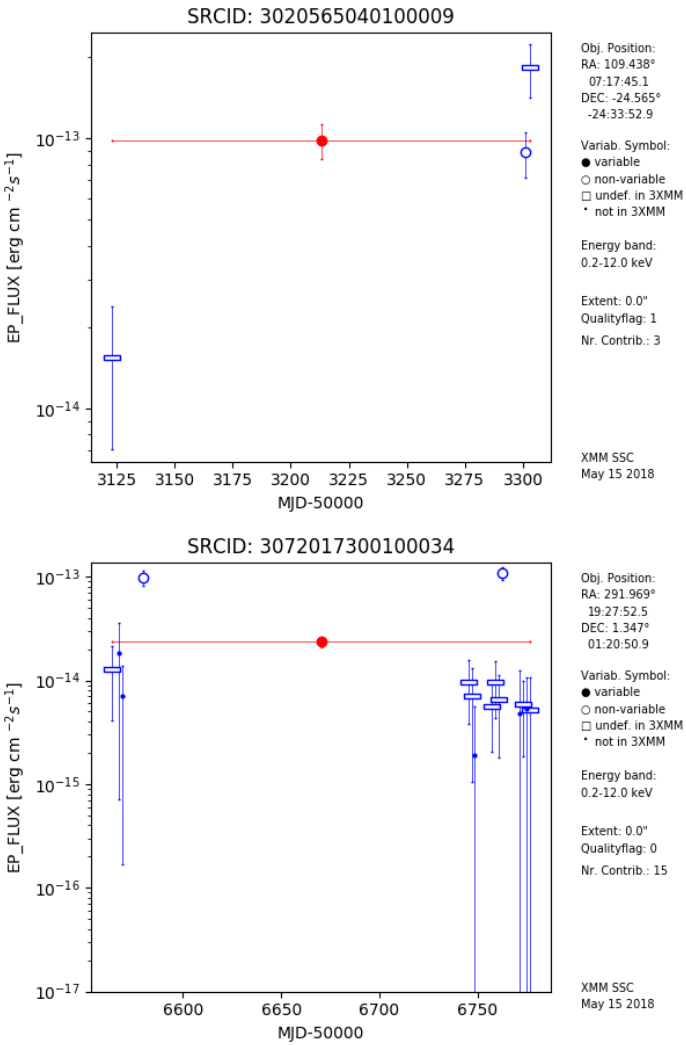

Fig. 17. Example light curves of candidates for long-term variability in the stacked catalogue, produced as auxiliary catalogue products. The objects have no counterpart with SDSS classification within 5″, and their 3XMM-DR7 counterpart is not known to be short-term variable. Plot symbols inform about short- and long-term variability and non-detections in 3XMM-DR7 and are explained in Appendix B.3.

to obtain DR7-specific information on the potential counterparts, for example on their short-term variability (Sect. 4.5), and to identify new stacked detections. For the sources in the stacked catalogue, the simultaneously fit coordinates RA and DEC with the pure statistical position error RADEC_ERR are used in the match, and for the unique 3XMM-DR7 sources their combined astrometrically corrected positions SC_RA and SC_DEC with the combined statistical and systematic error SC_POSERR. Two sources are associated if their separation is no larger than three times the sum of their position errors, which is assumed to be at least one arcsecond to account for systematic errors. The matching radius per source is thus $r_{\mathrm{match}} = \max(1'', 3 \times [\mathrm{RADEC\_ERR}_{\mathrm{stack}} + \mathrm{SC\_POSERR}_{\mathrm{3XMM\_DR7}}])$.

63 788 3XMM-DR7 counterparts of stacked sources are found, part of them at large separations owing to large position errors in one of the catalogues, and their contributing 3XMM-DR7 detections are identified. The associated 3XMM-DR7 sources are included in the stacked catalogue with their identifiers, coordinates, and short-term variability information where available. The combined parameters of the unique source are copied from the 3XMM-DR7 catalogue of sources to the stacked

Table 3. Cross-matches of the sources in the stacked catalogue: best X-match within a matching radius of 5″, given in total numbers in the column labelled "Matches" and as percentage of the 71 951 stacked catalogue sources in the column labelled "Share".

Catalogue	Matches	Share	Ref.
2MASS	16 859	23.4 %	(1)
AllWISE	40 163	55.8 %	(2)
GALEX GR5 AIS	6 609	9.2 %	(3)
UKIDSS DR9 LAS	8 208	11.4 %	(4)
NOMAD	31 628	44.0 %	(5)
Pan-STARRS1	36 995	51.4 %	(6)
SDSS DR12	21 887	30.4 %	(7)
Gaia DR2	28 321	39.4 %	(8)
Chandra CSC 2.0 (pre-release)	13 771	19.1 %	(9)

References. (1) Skrutskie et al. (2006); (2) Cutri & et al. (2014); (3) Bianchi et al. (2011); (4) Lawrence et al. (2007); (5) Zacharias et al. (2004); (6) Chambers et al. (2016); (7) Blanton et al. (2017); (8) Gaia Collaboration et al. (2018); (9) Evans et al. (2010).

source row. The parameters of each contributing 3XMM-DR7 detection found in an observation that is part of the stacked catalogue are copied from the 3XMM-DR7 catalogue of detections to the corresponding row per observation in the stacked catalogue. This applies to 117 125 individual 3XMM-DR7 detections in total. The observation-level values of the 3XMM-DR7 associated columns remain undefined if the 3XMM-DR7 source has not been detected in the respective observation. The offset between the source in the stacked catalogue and the associated 3XMM-DR7 source is given in the catalogue column DIST_3XMMDR7 in the stacked source rows, and the offset between the stacked source and the contributing 3XMM-DR7 detection in the respective row per observation, if applicable. It can be used to set a distance cut and restrict the maximum separation between associated sources.

The parameters of associated stacked and 3XMM-DR7 sources are generally consistent with each other within a few percent, which is within their uncertainties. The median all-EPIC flux of all sources with a 3XMM-DR7 association, for example, is 1.97×10^{-14} erg cm^{-2} s^{-1} and their median flux error is 6.89×10^{-15} erg cm^{-2} s^{-1}. The median SC_EP_8_FLUX of the 3XMM-DR7 counterparts is 1.78×10^{-14} erg cm^{-2} s^{-1} and the median error SC_EP_8_FLUX_ERR 5.96×10^{-15} erg cm^{-2} s^{-1}, including sources with different numbers of contributing observations in the stacked catalogue and in 3XMM-DR7. For the detections per observation, a median flux of 2.06×10^{-14} erg cm^{-2} s^{-1} and a median flux error 9.17×10^{-15} erg cm^{-2} s^{-1} is derived from the stacked fits, compared to a median 3XMM-DR7 flux of 2.09×10^{-14} erg cm^{-2} s^{-1} and flux error of 8.73×10^{-15} erg cm^{-2} s^{-1}.

Within the subset of observations that have entered the stacked catalogue, 128 509 individual detections are listed in the 3XMM-DR7 catalogue. Including detections from other observations of multiply observed fields, they have been merged into 73 784 unique sources. In the positional match between 3XMM-DR7 and the stacked catalogue within three times the position errors, 63 788 unique 3XMM-DR7 sources are found as potential counterparts to sources in the stacked catalogue, while the other 3XMM-DR7 detections are not recovered by stacked source detection. In addition to the differences between source detection on single and on multiple observations discussed in Sect. 4.3, the background maps for 3XMM-DR7 were created using spline fits, those for the stacked catalogue by the new adaptive smooth-

ing method. The different background treatment affects the net counts of tentative sources and thus their detection likelihood. Photons can be distributed slightly differently because of the different spatial binning, resulting from the different image sizes used in the two catalogues, which causes fluctuations close to the detection likelihood limit. A detailed discussion on how different source-detection runs and different background values can affect the final source selection is given in Paper VII. In addition, the percentage of poor detections among the missing 3XMM-DR7 sources is above the catalogue average. 90.7 % of the 73 784 unique sources in the 3XMM-DR7 subset have a good quality flag SUM_FLAG_3XMMDR7 of 0 or 1. Among the not recovered sources, 80.4 % have a flag of 0 or 1, while 19.6 % have a flag of 2 or more, indicating poor detection quality owing to complexities in the environment of the source. For the individual contributing detections, the effect is even more prominent: 95 % of all detections in the 3XMM-DR7 subset have a quality flag of 0 or 1, but only 81.7 % of the not recovered detections.

8 163 sources in the stacked catalogue do not have a counterpart in 3XMM-DR7 and are thus new findings, 7 624 (93.4 %) of them having a quality flag STACK_FLAG of 0 or 1. If the separation between sources in the stacked catalogue and 3XMM-DR7 associations is more conservatively restricted to a maximum of 15″, the numbers increase to 8 458 new sources and 7 906 with a good quality flag. More than 60 % of them have a tentative counterpart in one of the infra-red and optical catalogues listed in Table 3, described at the end of this section.

When comparing the source parameters in the two catalogues, the differing methods used to derive them should be kept in mind. All values in the stacked catalogue are fitted simultaneously or directly derived from the stacked fit, while individual 3XMM-DR7 detections are matched to compile the 3XMM-DR7 catalogue of unique sources. In particular, the stacked source coordinates are fitted simultaneously, while the merged coordinates of the 3XMM-DR7 unique sources are weighted means of the individually fitted coordinates of the contributing detections. 3XMM-DR7 fields are astrometrically rectified by comparing them with optical and infra-red catalogues before the coordinates are merged. The values given in the RADEC_ERR columns of the stacked and the 3XMM catalogues are the statistical errors of the fit to the positions, while the merged 3XMM-DR7 SC_POSERR position errors include an additional component from the astrometric correction. Observations from which detections are merged into unique 3XMM-DR7 sources can be missing from the stacked catalogue because of the selection criteria of clean observations. Conversely, each selected observation in the stack is used to derive the source parameters irrespective of the detection likelihood during this observation, while a low-likelihood detection is not included in the 3XMM-DR7 catalogue and does not contribute to the merged unique source. Out of the 63 788 associated sources, only 26 704 thus have the same number of contributing observations in both catalogues, while 28 070 have more and 9 014 have fewer contributions in the stacked catalogue than in 3XMM-DR7.

The stacked catalogue has been also cross-matched with a selection of external optical and infra-red catalogues and the pre-release version of the Chandra CSC 2.0 using the X-Match service of the Centre de Données astronomiques de Strasbourg (Pineau et al. 2011). The best match within a radius of 5″ is chosen. Table 3 gives the number of matches and their percentage with respect to the stacked catalogue. 57 268 or 80 % of the sources have a tentative optical or infra-red counterpart, 59 227 one in any of the selected catalogues including CSC 2.0.

4.7. Caveats

Several limitations to this first stacked catalogue are identified and described throughout the paper.

The catalogue is based on a selection of good-quality observations. In particular, repeated observations of a field have not entered the stacked catalogue if they have been attributed a 3XMM-DR7 OBS_CLASS above 2.

The detection likelihoods, calculated as the mathematical equivalent of a two-parameter fit, can be low if very few source counts are distributed across many images, and faint sources may be lost for purely statistical reasons. The effect is largely compensated by the refined box-detection strategy and source-selection criteria used to construct the stacked catalogue.

Although the number of spurious detections is likely reduced by stacked source detection with respect to the individual observations, spurious detections for example along instrumental features, stray light, or residuals in the PSF fit to bright sources have entered the catalogue. They are partly due to the more flexible criterion of a sufficiently high detection likelihood during at least one contributing observation to transfer a detection to the catalogue. Many of them can be identified by visual inspection of the images. A filtering expression on a total detection likelihood above six helps to further decrease the amount of potentially spurious detections at the expense of losing transient sources.

The source quality flags are purely derived by the automated quality assessment of a modified version of the task `dpssflag` without visual screening. They warn the users about low detector coverage of a source, possible source confusion, a source position on known bad pixels, and possible extended spurious sources. Auxiliary images published together with the catalogue offer the opportunity to inspect the detection area of the sources.

No astrometric correction has been applied to the measured source positions. Their mean systematic error is estimated to be 0.43″ up to 0.74″, depending on its definition. This astrometric accuracy is better than that of uncorrected source positions listed in the 2XMM and 3XMM catalogues.

High-proper motion objects are not uniquely recovered by stacked source detection, because the algorithm is not designed to follow position changes between observations. They show up as several seemingly long-time variable objects in the catalogue and need to be identified manually or via comparison with astrometric catalogues.

4.8. Access to the catalogue and auxiliary products

The catalogue table is compiled as one file in the Flexible Image Transport System (FITS) format and can be downloaded directly from the website of the XMM-Newton SSC[6]. It also provides the catalogue documentation and links to the other resources[7]. The associated list of observations, also delivered in FITS format, informs about all selected OBS_IDs, their assignment to stacks, the area covered, the exposure time ratio to the longest observation in the stack, and the setup of the observation including the filters chosen per instrument. Web-based user interfaces to the catalogue and the associated auxiliary products are provided by the XCatDB[8] and ESA's XMM-Newton Science Archive (XSA[9]). The catalogue will also be included in the VizieR and HEASARC data services.

[6] `http://xmmssc.irap.omp.eu`
[7] `http://xmmssc.irap.omp.eu/Catalogue/3XMM-DR7s/3XMM_DR7stack.html`
[8] `https://xcatdb.unistra.fr/3xmmdr7s/`
[9] `https://www.cosmos.esa.int/web/xmm-newton/xsa`

For all sources in the catalogue, auxiliary products are created: broad-band X-ray images in the 0.2−12.0 keV energy band, false-colour RGB images within 0.2 − 1.0 keV, 1.0 − 2.0 keV, and 2.0 − 12.0 keV, corresponding to the energy bands 1 plus 2, 3, and 4 plus 5, and optical finding charts from the highest-quality image out of Pan-STARRS G (Chambers et al. 2016), skyMapper G (Wolf et al. 2018), and ESO Online Digitized Sky Survey DSS2[10] blue and red band. All images are centred on the source position in the stacked catalogue. The X-ray and RGB images show a section of the mosaics, which are created from all observations in a stack using the task `emosaic`, and cover $10' \times 10'$. Information on source extent and quality flag are included. The optical finding charts have a side length of $2'$. For all sources that were observed at least twice with non-zero counts, long-term light curves are constructed from the mean all-EPIC fluxes in the stack and each contributing observation. Short-term variability according to 3XMM-DR7 is indicated in the plots if a counterpart has been found.

Details on the long-term light curves and on the construction of the optical finding charts are given in Sect. B.3 of the Appendix. Figure B.1 shows a complete set of the auxiliary products for an arbitrarily chosen source.

5. Summary and conclusions

The first serendipitous source catalogue from overlapping XMM-Newton observations contains 71 951 unique sources in 1 789 observations, taken between 2000 and 2016 and grouped into 434 stacks. Its processing is based on a new module, using existing, improved, and new source-detection code, which is distributed as part of the XMM-Newton Science Analysis System. Stacked source detection proves to be more sensitive to faint sources and likely results in a lower false-positive rate than source detection on the individual observations. Source parameters are determined with higher accuracy, and the catalogue can be used in particular to investigate faint sources and potentially variable sources. More than 8 000 catalogue sources are new detections with respect to 3XMM-DR7. At least 60 % of them have tentative counterparts in other catalogues within $5''$.

The stacked catalogue gives information on the parameters of each source in the stack of observations as well as in its contributing observations and on long-term flux variability directly from the fitting process. Post-processing quality assessment is automatically applied to all sources. An accompanying list of observations includes their technical details like the observation date and the filters used. The auxiliary source images can be accessed via the XSA interface to the stacked catalogue.

Providing information on source detection and catalogue construction, this paper is intended to be the reference for this and subsequent releases of stacked catalogues. The future releases are envisaged to be based on less restrictive selection criteria of observations to be included in the stacks than used for this first edition. The next release is planned to provide upper-limit flux estimates at the source positions. Methods to apply astrometric corrections to the individual observations before performing stacked source detection will be investigated to further improve its sensitivity.

Acknowledgements. SSC work at AIP has been supported by Deutsches Zentrum für Luft- und Raumfahrt (DLR) through grants 50 OX 1401, 50 OX 1701, and 50 OR 1604. We greatly appreciate the fruitful collaboration with the colleagues at ESA's XMM-Newton Science Operations Centre (SOC) and the kind support by the IT service team at the AIP. NW, MC and FK acknowledge the CNES support. This project has made use of CDS services, CDS, Strasbourg, France, of FTOOLS by NASA's HEASARC (Blackburn 1995), and of TOPCAT/stilts (Taylor 2005).

[10] `https://archive.eso.org/dss/dss`

References

Bianchi, L., Herald, J., Efremova, B., et al. 2011, Ap&SS, 335, 161
Blackburn, J. K. 1995, in ASP Conf. Ser. Vol. 77, Astronomical Data Analysis Software and Systems IV, ed. R. A. Shaw, H. E. Payne, & J. J. E. Hayes, 367
Blanton, M. R., Bershady, M. A., Abolfathi, B., et al. 2017, AJ, 154, 28
Cash, W. 1976, A&A, 52, 307
Cash, W. 1979, ApJ, 228, 939
Chambers, K. C., Magnier, E. A., Metcalfe, N., et al. 2016, ArXiv e-prints [arXiv:1612.05560]
Cutri, R. M. & et al. 2014, VizieR Online Data Catalog, 2328
De Luca, A., Salvaterra, R., Tiengo, A., et al. 2016, The Universe of Digital Sky Surveys, 42, 291
Evans, I. N., Primini, F. A., Glotfelty, K. J., et al. 2010, ApJS, 189, 37
Fernique, P., Allen, M., Boch, T., et al. 2017, HiPS - Hierarchical Progressive Survey Version 1.0, IVOA Recommendation 19 May 2017
Fernique, P., Boch, T., Donaldson, T., et al. 2014, MOC - HEALPix Multi-Order Coverage map Version 1.0, IVOA Recommendation 02 June 2014
Fernique, P., Oberto, A., Boch, T., & Bonnarel, F. 2010, in Astronomical Society of the Pacific Conference Series, Vol. 434, Astronomical Data Analysis Software and Systems XIX, ed. Y. Mizumoto, K.-I. Morita, & M. Ohishi, 163
Gabriel, C., Denby, M., Fyfe, D. J., et al. 2004, in ASP Conf. Ser. Vol. 314, Astronomical Data Analysis Software and Systems (ADASS) XIII, ed. F. Ochsenbein, M. G. Allen, & D. Egret, 759
Gaia Collaboration, Brown, A. G. A., Vallenari, A., et al. 2018, ArXiv e-prints [arXiv:1804.09365]
Jansen, F., Lumb, D., Altieri, B., et al. 2001, A&A, 365, L1
Lawrence, A., Warren, S. J., Almaini, O., et al. 2007, MNRAS, 379, 1599
Lin, D., Webb, N. A., & Barret, D. 2012, ApJ, 756, 27
Mateos, S., Saxton, R. D., Read, A. M., & Sembay, S. 2009, A&A, 496, 879
Page, M. J., Brindle, C., Talavera, A., et al. 2012, MNRAS, 426, 903
Pineau, F.-X., Boch, T., & Derriere, S. 2011, in Astronomical Society of the Pacific Conference Series, Vol. 442, Astronomical Data Analysis Software and Systems XX, ed. I. N. Evans, A. Accomazzi, D. J. Mink, & A. H. Rots, 85
Plucinsky, P. P., Beardmore, A. P., Foster, A., et al. 2017, A&A, 597, A35
Read, A. M., Guainazzi, M., & Sembay, S. 2014, A&A, 564, A75
Read, A. M. & Ponman, T. J. 2003, A&A, 409, 395
Rosen, S. R. & Read, A. M. 2017, The EXTraS long-term Variability Catalogue, EXTraS Public Data Archive Documentation FP7-SPACE-2013-1 GA n.607452
Rosen, S. R., Webb, N. A., Watson, M. G., et al. 2016, A&A, 590, A1
Saxton, R. D., Read, A. M., Esquej, P., et al. 2008, A&A, 480, 611
Skrutskie, M. F., Cutri, R. M., Stiening, R., et al. 2006, AJ, 131, 1163
Stewart, I. M. 2009, A&A, 495, 989
Strüder, L., Briel, U., Dennerl, K., et al. 2001, A&A, 365, L18
Taylor, M. B. 2005, in ASP Conf. Ser. Vol. 347, Astronomical Data Analysis Software and Systems XIV, ed. P. Shopbell, M. Britton, & R. Ebert, 29
Turner, M. J. L., Abbey, A., Arnaud, M., et al. 2001, A&A, 365, L27
Watson, M. G., Auguères, J.-L., Ballet, J., et al. 2001, A&A, 365, L51
Watson, M. G., Schröder, A. C., Fyfe, D., et al. 2009, A&A, 493, 339
Wenger, M., Ochsenbein, F., Egret, D., et al. 2000, A&AS, 143, 9
Wolf, C., Onken, C. A., Luvaul, L. C., et al. 2018, PASA, 35, e010
Zacharias, N., Monet, D. G., Levine, S. E., et al. 2004, in Bulletin of the American Astronomical Society, Vol. 36, American Astronomical Society Meeting Abstracts, 1418

Appendix A: The automated method used to identify high-background fields

To establish a high-background threshold for each EPIC instrument from a large sample of exposures, a mean background count rate per unit area between 0.2 and 12.0 keV is determined for each of the about 8 000 3XMM-DR7 EPIC observations taken in full-frame or large-window mode in the following way. From the event lists pre-filtered with the 3XMM GTIs, "cheesed" images are created per instrument by excluding circular regions around known 3XMM-DR7 sources with the radius being the maximum of *(i)* 30″, *(ii)* the square root of the counts as a rough approximation to PSF scaling, and *(iii)* – if the source has a summary flag of 0 or 1 in 3XMM-DR7 indicating a good-quality detection – the source extent. For bright sources with an EPIC/pn count rate above 1 count s^{-1}, summed over all five energy bands, stripes along the readout direction are excluded to get rid of out-of-time events. To simplify the procedure, the stripes have a constant width of 40″ over the whole chip extent. Corresponding cheesed masks are derived from the cheesed images, which give the valid pixels per instrument during the observation.

The averaged background count rate per area in units of cts $arcsec^{-2}$ s^{-1} in each cheesed image is the total number of photons divided by the number of pixels in the cheesed mask, the pixel size in square arcseconds, and the net exposure time in seconds. For EPIC-pn, the four quadrants of the chip are treated separately, because they are independent of each other and can have different lifetimes and thus background levels, in particular if they are operated in continuous counting mode while the telemetry of the instruments is saturated and data are transmitted incompletely and unusable for scientific analyses. The maximum background value of the quadrants is used as a measure of the whole observation.

The method has two general limitations. *(i)* It does not distinguish between high sky background and emission of very extended sources within the field of view. Both scenarios are considered problematic for (stacked) source detection and treated in the same way. *(ii)* Since the count rate is calculated as an average over the chip or chip quadrants, background features that are prominent on small scales only like stray light are not reliably flagged by this method. A measure of spatial background variability over the field of view can be used to identify these cases, but has not been implemented so far.

The distributions of mean background values are shown in Fig. A.1 for each EPIC instrument. Observations that have a HIGH_BACKGROUND flag in 3XMM-DR7 are plotted in red, with a zoom to high rates in the inset. The 3XMM flag is set for the whole observation if at least one instrument experienced increased background. In the plots per instrument of Fig. A.1, some observations with a low mean background level in one instrument are therefore marked in red owing to a 3XMM-DR7 background flag triggered by one of the other instruments. The height of the peak in the histograms is estimated from a fit with an empirically chosen Lorentz function $l(r) = h/((r-c)^2/w^2+1)$ with count rate r, peak centre c, height h, and half width at half maximum w, omitting the left wing of the peak. It translates into a cumulative Half Cauchy probability distribution $2\arctan((\log_{10}(r) - c)/w)/\pi$, regarding values left of the peak as low background with probability zero. Thus, the background count rate per area of each individual exposure can be converted into a probability that the exposure may be affected by high background emission. For the stacked catalogue, a probability cut of 87 % was used to exclude high-background observations from stacked source detection (Sect. 3.1).

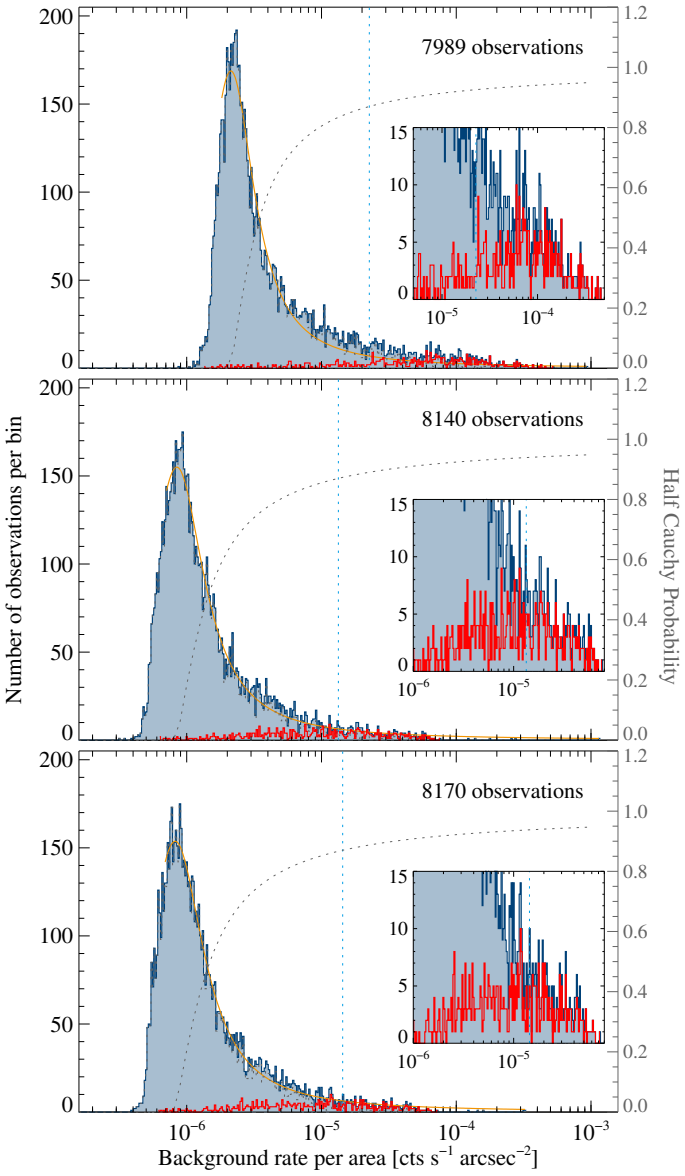

Fig. A.1. Histograms of the derived background rates per area of all considered observations of EPIC-pn, MOS1, and MOS2 (from top to bottom). The orange line shows the Lorentz fit to the histogram and the grey dashed line the Half Cauchy probability distribution, with the scale given in the right axis. The dashed vertical line marks the 87 % probability cut used to discard observations as high-background contaminated. The red histogram shows the distribution of observations that have a HIGH_BACKGROUND flag in 3XMM-DR7 for comparison. *Insets:* zoom to the highest background values.

Appendix B: Auxiliary information on the stacked catalogue and its selection of observations

Appendix B.1: Proposal categories included in the catalogue

Table B.1 lists the number of catalogue observations per XMM-Newton proposal category. Most of the 3XMM-DR7 observations comprising objects with large extent have been de-selected from the first stacked catalogue.

Table B.1. XSA proposal categories of the selected observations.

XSA proposal category		number
A	Stars, White Dwarfs and Solar System	382
B	White Dwarf Binaries, Neutron Star Binaries, Cataclysmic Variables, ULX and Black Holes	192
C	Supernovae, Supernova Remnants, Diffuse Emission, Diffuse galactic Emission and Isolated Neutron Stars	119
D	Galaxies, Galactic Surveys and X-ray Background	111
E	Galaxies, Groups of Galaxies, Clusters of Galaxies and Superclusters	229
F	Active Galactic Nuclei, Quasars, BL-Lac Objects and Tidal Disruption Events	291
G	Groups of Galaxies, Clusters of Galaxies and Superclusters	162
H	Cosmology, Extragalactic Deep Fields and Large Extragalactic Areas	303

Appendix B.2: Catalogue columns

Table B.2 gives an overview of all columns included in the catalogue and a short description of how the stacked parameters and the parameters per contributing observation are calculated. Entries centred within the two columns for stacked and observation-level values are valid for both of them. "*Null*" stands for undefined values / not-a-number, "zero" for 0.0. Weighted means of values x_i with errors σ_i are calculated as $\bar{x} = (\sum_{i=0}^{n} x_i/\sigma_i^2)/\sigma_x^2$ with $\sigma_x^2 = 1/\sum_{i=0}^{n} \sigma_i^{-2}$. Values copied from the nearest 3XMM-DR7 source within a matching radius of three times the summed position errors are labelled by the suffix _3XMMDR7.

Appendix B.3: Auxiliary products

The optical finding charts have been generated in three steps using tools based on the HiPS standard (Fernique et al. 2017) initially designed by the Astronomical Data Center (CDS) of the Observatoire de Strasbourg and adopted by the Virtual Observatory. The procedure makes use of a huge collection of multi-order coverage maps (Fernique et al. 2014) describing the sky coverage of many surveys and catalogues, which is operated by the CDS. The list of the HiPS surveys covering the position is requested from this database. The optical survey having the highest priority is selected and transmitted to an Aladin instance (Fernique et al. 2010) running behind a Tomcat server. This service gets the HiPS tiles covering the requested region from a CDS server and converts them into a FITS image. The operations are controlled by a Java client which runs an IDL[11] task written to produce the PDF file lastly. The image cuts are tuned to highlight the fainter features. The IDL code is derived from the Astronomical Catalogue Data Subsystem ACDS task of the XMM-Newton pipeline.

The long-term light curves are created for sources with non-zero counts during at least two observations and include the stacked EPIC flux value and the EPIC fluxes during the contributing observations. Different plot symbols are used to indicate tentative short- and long-term variability. The stacked flux is plotted with a filled circle, if the variability VAR_PROB of the source fluxes to be consistent with constant flux is 1 % or lower. Probabilities of short-term variability are included in 3XMM-DR7 for detections with at least 100 counts and indicated in the long-term light curves by the plot symbols of the fluxes calculated for each observation in the stacked catalogue. The flux is plotted with a filled circle, if a 3XMM-DR7 observation has been associated with the source in the stacked catalogue (cf. Sect. 4.6) and if its short-term variability flag VAR_FLAG_3XMMDR7 is true. Open circles are used in the opposite cases for tentatively non-variable sources. An open box of arbitrary size means that too few counts were collected during the observation to derive information on short-term variability in 3XMM-DR7, and a small dot that no 3XMM-DR7 detection has been associated with the source.

Figure B.1 shows them for an example source detected in nine stacked observations.

[11] Based on proprietary Interactive Data Language software, `https://www.harrisgeospatial.com/SoftwareTechnology/IDL.aspx`.

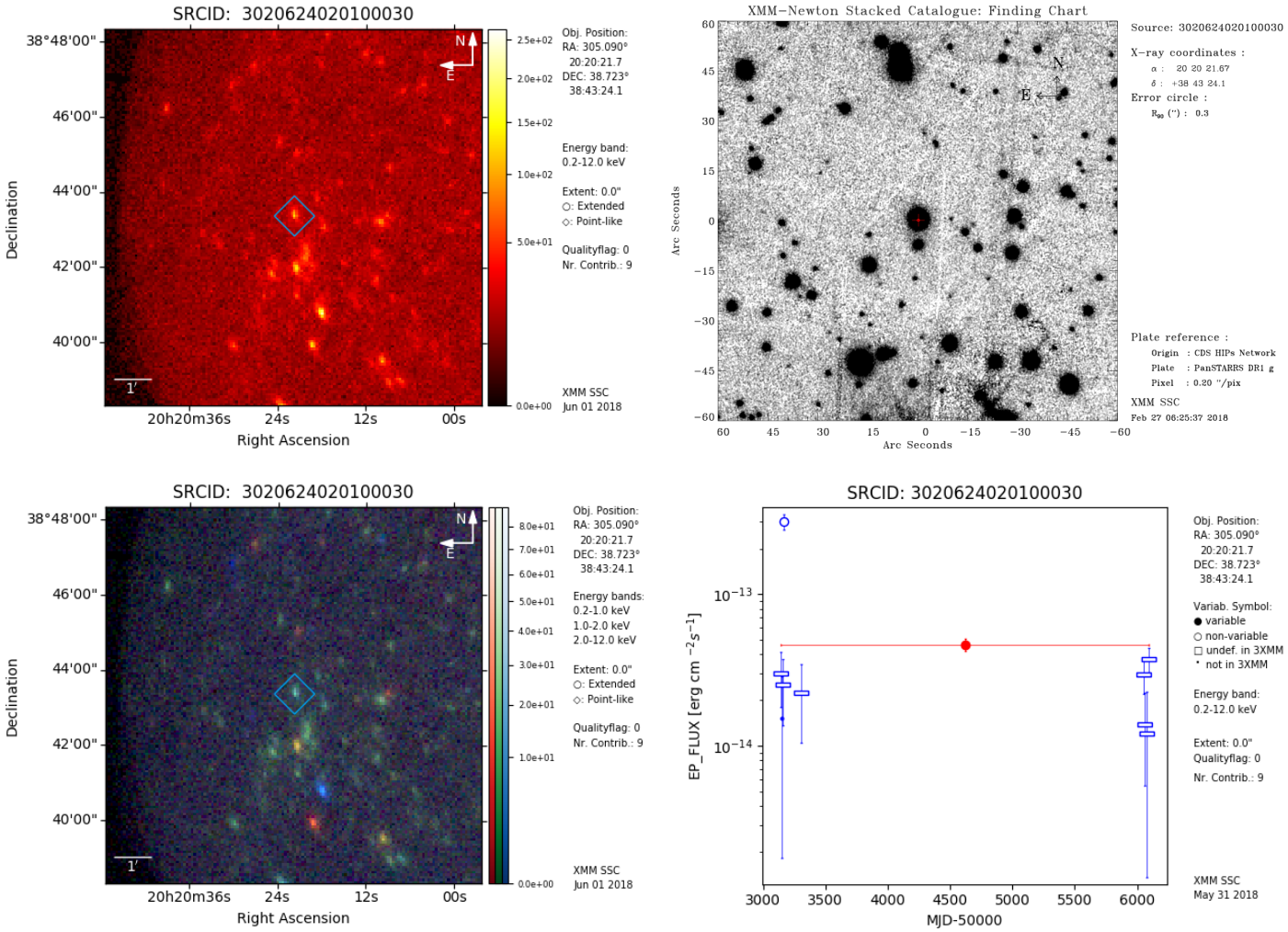

Fig. B.1. Examples of the auxiliary products accompanying each catalogue source: broad-band X-ray image, false-colour RGB image of three X-ray energy bands, optical finding chart, and long-term light curve.

Table B.2. Description of all catalogue columns. The table column "Stack" comprises a short summary of how the parameter value in the summary row per stack is calculated, "Observation" of the value derived for the individual contributing observation. Values per instrument are labelled by *CC*, which stands for one of PN, M1, M2. The energy bands, defined as for 3XMM, are abbreviated by $1 \leq n \leq 5$ and for the hardness ratios by $1 \leq i \leq 4$. Broad-band EPIC values are derived in the 0.2−12.0 keV range.

Column name	Format	Unit	Description	Observation	Stack
Columns 1−4: Detection characteristics					
SRCID	long		Identifier of the detection.	Assigned to all rows per source	
OBS_ID	string		XMM-Newton observation identifier.	Per observation	*null*
N_OBS	integer		Number of observations involved in the stack.	*null*	Per stack
N_CONTRIB	integer		Number of observations in which the source was fitted.	*null*	Per stack
Columns 5−15: Coordinates and associated identifier					
RA	double	degrees	Right ascension (J2000).	Combined fit	
DEC	double	degrees	Declination (J2000).	Combined fit	
RADEC_ERR	float	arcsec	Square root of the sum of the squared 1σ errors in X_IMA and Y_IMA $\sqrt{\sigma^2_{\mathrm{X\_IMA}} + \sigma^2_{\mathrm{Y\_IMA}}}$, converted to arcsec.	Combined fit	
LII	double	degrees	Galactic longitude.	Combined fit	
BII	double	degrees	Galactic latitude.	Combined fit	
X_IMA(_ERR)	float	pixel	X coordinate within the re-binned image and its 1σ error. Image pixels are binned to $4'' \times 4''$.	Combined fit	
Y_IMA(_ERR)	float	pixel	Y coordinate within the re-binned image and its 1σ error. Image pixels are binned to $4'' \times 4''$.	Combined fit	
DIST_NN	float	arcsec	Distance to the nearest neighbouring detection.	Combined fit	
SRCNAME	string		Source name in the style of the 3XMM IAU names, ending on an "s" for stacked detection.	Assigned to all rows per source	
Columns 16−23: 3XMM counterpart: values copied from 3XMM-DR7					
IAUNAME_3XMMDR7	string		IAU name assigned to the nearest unique source in 3XMM-DR7.	Assigned to all rows per source with a 3XMM-DR7 counterpart	
SRCID_3XMMDR7	long		Unique source identifier of the nearest source in 3XMM-DR7 within a correlation radius of three times the sum of the position errors. *Null*, if no counterpart is found.	Assigned to all rows per source with a 3XMM-DR7 counterpart	
DETID_3XMMDR7	long		Identifier of the 3XMM-DR7 per-observation detection that contributes to the unique source SRCID_3XMMDR7, if existing.	Per OBS_ID	*null*
RA_3XMMDR7	double	degrees	Mean right ascension of the unique 3XMM-DR7 source and its contributing detections after field rectifications.	RA of DETID_3XMMDR7	SC_RA of SRCID_3XMMDR7
DEC_3XMMDR7	double	degrees	Mean declination of the unique 3XMM-DR7 source and its contributing detections after field rectifications.	DEC of DETID_3XMMDR7	SC_DEC of SRCID_3XMMDR7
POSERR_3XMMDR7	float	arcsec	Position error of the unique 3XMM-DR7 source and its contributing detections, including the error derived from the field rectification.	POSERR of DETID_3XMMDR7	SC_POSERR of SRCID_3XMMDR7
DIST_3XMMDR7	double	arcsec	Distance between the source and the nearest unique source / its contributing detection in 3XMM-DR7.	Distance to DETID_3XMMDR7	Distance to SRCID_3XMMDR7
NDETECT_3XMMDR7	integer		Number of DR7 detections N_DETECTIONS of the nearest unique source in 3XMM-DR7.	*null*	Of SRCID_3XMMDR7

Table B.2. Continued.

Column name	Format	Unit	Description	Observation	Stack
Columns 24–71: Fluxes					
EP_FLUX	float	erg cm^{-2} s^{-1}	All-EPIC flux between 0.2 and 12 keV: dead-time corrected count rates in the entire PSF, multiplied with the respective energy conversion factors. *Null*, if the exposure is zero, like on chip gaps, or if the covered PSF fraction is below 15 %.	Mean of the instrument fluxes weighted by the inverse squared errors	
EP_FLUX_ERR	float	erg cm^{-2} s^{-1}	1σ error on EP_FLUX.	Inverse square root of the sum of inverse squared errors per instrument	
EP_*n*_FLUX(_ERR)	float	erg cm^{-2} s^{-1}	All-EPIC flux and 1σ flux error in energy band *n*. *Null*, if the exposure is zero or if the covered PSF fraction is below 15 %. Zero with non-zero errors, if no counts are detected in spite of sufficient PSF coverage.	Mean of the instrument values weighted by the inverse squared errors	
*CC*_FLUX(_ERR)	float	erg cm^{-2} s^{-1}	Total flux and 1σ flux error in instrument *CC*. *Null* / zero as before.	Sum of fluxes and flux errors per energy band	
*CC*_*n*_FLUX(_ERR)	float	erg cm^{-2} s^{-1}	Flux and 1σ flux error per instrument *CC* and energy band *n*. *Null* / zero as before.	Fitted per input image	Mean of the observation-level values weighted by the exposure time
Columns 72–117: Count rates and count numbers					
EP_RATE	float	counts s^{-1}	All-EPIC count rate between 0.2 and 12.0 keV: background-subtracted and vignetting corrected count rate in the entire PSF. *Null*, if the exposure is zero or if the covered PSF fraction is below 15 %. Zero with non-zero errors, if no counts are detected in spite of sufficient PSF coverage.	Sum of the count rates per instrument	Mean of the observation-level rates weighted by the exposure time
EP_RATE_ERR	float	counts s^{-1}	1σ error on the count rate. *Null*, if the exposure is zero or if the covered PSF fraction is below 15 %.	Square root of the quadratic sum of the errors per instrument	Combined observation-level errors weighted by the exposure time
*CC*_RATE(_ERR)	float	counts s^{-1}	Total count rate and count-rate error in instrument *CC*. *Null* / zero as before.	Sum of the values per energy band	Mean of the observation-level values weighted by the exposure time
*CC*_*n*_RATE(_ERR)	float	counts s^{-1}	Count rate and count-rate error per instrument *CC* and energy band *n*. *Null* / zero as before.	Fitted per input image	Mean of the observation-level values weighted by the exposure time
EP_CTS	float	counts s^{-1}	All-EPIC counts: background-subtracted source counts in the entire PSF. *Null*, if the exposure is zero or if the covered PSF fraction is below 15 %.	Sum of the source counts per instrument	
EP_CTS_ERR	float	counts s^{-1}	1σ error on the counts. *Null*, if the exposure is zero or if the covered PSF fraction is below 15 %.	Square root of the quadratic sum of the errors per instrument	
*CC*_CTS(_ERR)	float	counts s^{-1}	Total counts and error in instrument *CC*.	Sum of the values per energy band	
Columns 118–139: Detection and extent likelihoods					
EP_DET_ML	float		Total equivalent maximum detection likelihood, normalised to two degrees of freedom.	Calculated from all valid contributing images	

Table B.2. Continued.

Column name	Format	Unit	Description	Observation	Stack
*CC*_DET_ML	float		Equivalent maximum detection likelihood for instrument *CC*, normalised to two degrees of freedom.	Calculated from all valid contributing images per instrument	
*CC*_*n*_DET_ML	float		Equivalent maximum detection likelihood per instrument *CC* and energy band *n*, normalised to two degrees of freedom.	Value per input image	Calculated from all valid contributing images per instrument and energy band
EXTENT	float	arcsec	Source extent radius, derived from the model source PSF convolved with a beta profile. Below an extent of 6″, it is considered unresolved and set to zero, the source is "point-like".	Combined fit	
EXTENT_ERR	float	arcsec	1σ error on the source extent radius. *Null*, if the extent radius is below 6″.	Combined fit	
EXTENT_ML	float		Likelihood that the source is extended with radius EXTENT. *Null*, if the source is considered point-like.	Combined fit	
Columns 140–171: Hardness ratios					
EP_HR*i*	float		Equivalent all-EPIC hardness ratios $(r_{i+1} - r_i)/(r_{i+1} + r_i)$ between the count rates r in energy bands i and $i + 1$.	Mean of all active instruments	
EP_HR*i*_ERR	float		1σ error on hardness ratio EP_HR*i*.	Error propagation of the contributing values	
*CC*_HR*i*(_ERR)	float		Hardness ratios $(r_{i+1} - r_i)/(r_{i+1} + r_i)$ between the count rates r in energy bands i and $i + 1$ per instrument.	Per input images	Mean of the observations
Columns 172–233: Fit characteristics					
*CC*_EXP	float	seconds	Exposure map values per instrument *CC*, including vignetting effects. The effective good exposure time is given in the ONTIME columns, described below.	Sum of the contributing images	
*CC*_*n*_EXP	float	seconds	Exposure map values per instrument *CC* and energy band.	Fitted per input image	Sum of the contributing images
*CC*_BG	float	cts px^{-1}	Background model at the central position of the source on the CCD. *Null*, if the exposure map is zero and if the centre of the source is located on a bad chip area.	Sum of all contributing images	
*CC*_*n*_BG	float	cts px^{-1}	Background model in energy band *n* at the CCD position of the source.	Sum of all valid images in energy band *n*	
EP_ONTIME	float	seconds	Total good exposure time at the central position of the source on the CCD. Zero, if the centre of the source is located on a bad chip area.	Maximum of the good exposure time per instrument	Sum of the maximum ontimes of all observations
*CC*_ONTIME	float	seconds	Total good exposure time of instrument *CC* at the CCD position of the source. Times are calculated by the task `evselect` and not vignetting corrected.	Read from the headers of the input files.	Sum of the observation-level values.
*CC*_MASKFRAC	float		Mean chip coverage in the detection mask per instrument, weighted by the point spread function of the source.	Minimum of the slightly differing values per energy band	Maximum of the observation-level values
EP_OFFAX	float	arcmin	Angular distance of the source to the boresight.	Minimum of the values per instrument.	*null*

Table B.2. Continued.

Column name	Format	Unit	Description	Observation	Stack
*CC*_OFFAX	float	arcmin	Angular distance of the source to the boresight in instrument *CC*.	Combined fit	*null*
*CC*_*n*_VIG	float		Vignetting fraction in instrument *CC* and energy band *n* at the central position of the source.	Read from the calibration data base	*null*
Columns 234–238: Quality flags					
STACK_FLAG	integer		Summarised quality flag of the detection. "0", if all flags are false. "1", if at least one of flags 1, 2, 3, 9 is true. "2", if at least one of flags 4 – 8 is true. "3", if STACK_FLAG is 2 for all contributing observations.	Numeric version of EP_FLAG	
EP_FLAG	string		Quality flags of the detection, automatically set and combined into a nine-characters string. A flag "true" means a warning on a detection condition.	Worst flag of all instruments	Worst flag of all observations
*CC*_FLAG	string		Quality flags in instrument *CC*.	Set per input image	Worst flag of all observations
Columns 239–268: Inter-observation variability of sources with at least two contributing observations					
VAR_CHI2	float		Reduced χ^2 of inter-observation flux variability in all contributing observations with valid non-zero fluxes.	*null*	$\frac{1}{n-1}\sum_{k=1}^{n}\left(\frac{F_k-F_{\rm EPIC}}{\sigma_k}\right)^2$
VAR_CHI2_*n*	float		Reduced χ^2 of inter-observation flux variability in energy band *n*.	*null*	
VAR_PROB	double		Probability that the measured flux values are consistent with constant inter-observation flux. The smaller VAR_PROB, the more likely the source shows inter-observation flux variability.	*null*	Derived from VAR_CHI2
VAR_PROB_*n*	double		Probability that the measured flux values are consistent with constant inter-observation flux in energy band *n*.	*null*	Derived from VAR_CHI2_*n*
FRATIO	float		Ratio between highest and lowest (non-zero, non-null) mean flux.	*null*	$F_{\rm max}/F_{\rm min}$
FRATIO_ERR	float		1σ error on the flux ratio.	*null*	$\left(\frac{\sigma^2_{F\rm min}}{F^2_{\rm min}}+\frac{\sigma^2_{F\rm max}}{F^2_{\rm max}}\right)^{0.5}\frac{F_{\rm max}}{F_{\rm min}}$
FRATIO_*n*(_ERR)	float		Ratio between highest and lowest mean flux in energy band *n* and its 1σ error.	*null*	
FLUXVAR	float		Largest difference between mean all-EPIC fluxes in terms of σ.	*null*	$\max_{k,l\in[1,n]}\frac{\lvert F_k-F_l\rvert}{\sqrt{\sigma_k^2+\sigma_l^2}}$
FLUXVAR_*n*	float		Largest difference between mean all-EPIC fluxes in terms of σ in energy band *n*.	*null*	
Columns 269–273: 3XMM-DR7 intra-observation variability of sources with a DR7 light curve					
CHI2PROB_3XMMDR7	double		EPIC χ^2 probability that the time series of the nearest unique source in 3XMM-DR7 is consistent with the source having constant flux during the observation.	EP_CHI2PROB in 3XMM-DR7	SC_CHI2PROB in 3XMM-DR7: Minimum of all contributing 3XMM-DR7 observations

Table B.2. Continued.

Column name	Format	Unit	Description	Observation	Stack
FVAR_3XMMDR7	double		Fractional variance of the nearest unique source in 3XMM-DR7.	FVAR in 3XMM-DR7 of the instrument with minimum CHI2PROB	SC_FVAR in 3XMM-DR7: Observation with minimum CHI2PROB
FVARERR_3XMMDR7	double		1σ error on FVAR_3XMMDR7.	FVAR_ERR in 3XMM-DR7 of the instrument with minimum CHI2PROB	SC_FVAR_ERR in 3XMM-DR7: Observation with minimum CHI2PROB
VAR_FLAG_3XMMDR7	boolean		Variability flag of the nearest unique source in 3XMM-DR7. True, if at least one exposure has CHI2PROB below 10^{-5}.	EP_VAR_FLAG in 3XMM-DR7	SC_VAR_FLAG in 3XMM-DR7: Observation with minimum CHI2PROB
SUM_FLAG_3XMMDR7	integer		Integer representation of the quality flags of the nearest 3XMM-DR7 source from automatic and visual screening.	SUM_FLAG in 3XMM-DR7	SC_SUM_FLAG in 3XMM-DR7
Columns 274–284: Observation characteristics					
MJD_FIRST	double	days	Modified Julian Date of the start of the observation (JD−2 400 000.5).	Read from the headers of the input files	First contributing observation
MJD_LAST	double	days	Modified Julian Date of the end of the observation (JD−2 400 000.5).	Read from the headers of the input files	Last contributing observation
PA_PNT	float	degrees	Mean position angle of the spacecraft during the observation.	File headers	*null*
REVOLUT	short		XMM-Newton orbit of the observation.	File headers	*null*
*CC*_SUBMODE	string		Observing mode of instrument *CC*.	File headers	*null*
*CC*_FILTER	string		Filter used during the observation.	File headers	*null*
URL_3XMMDR7	string		Web page of the nearest unique source in 3XMM-DR7.	Copied from 3XMM-DR7	